Prepared for submission to JHEP PITT-PACC 1909

Leptonic Scalars at the LHC

André de Gouvêa,[a] P. S. Bhupal Dev,[b] Bhaskar Dutta,[c] Tathagata Ghosh,[d] Tao Han,[e] Yongchao Zhang[b]

[a]*Department of Physics and Astronomy, Northwestern University, Evanston, IL 60208, USA*
[b]*Department of Physics and McDonnell Center for the Space Sciences, Washington University, St. Louis, MO 63130, USA*
[c]*Mitchell Institute for Fundamental Physics and Astronomy, Department of Physics and Astronomy, Texas A&M University, College Station, Texas 77843, USA*
[d]*Department of Physics and Astronomy, University of Hawaii, Honolulu, HI 96822, USA*
[e]*Pittsburgh Particle Physics, Astrophysics, and Cosmology Center, Department of Physics and Astronomy, University of Pittsburgh, 3941 O'Hara St., Pittsburgh, PA 15260, USA*

Abstract: We explore the neutrino non-standard interaction with leptonic scalars ϕ which are gauge-singlets and carry two units of lepton-number-charge. These leptonic scalars are forbidden from interacting with the Standard Model (SM) fermions at the renormalizable level and, if one allows for higher-dimensional operators, couple predominantly to SM neutrinos. For masses at or below the electroweak scale, ϕ decays exclusively into neutrinos. Its unique production signature at hadron collider experiments like the LHC would be via the vector boson fusion process and lead to same-sign dileptons, two forward jets in opposite hemispheres, and missing transverse energy, i.e., $pp \to \ell_\alpha^\pm \ell_\beta^\pm jj + E_T^{\rm miss}$ (α, $\beta = e, \mu, \tau$). Exploiting the final states of electrons and muons, we estimate, for the first time, the sensitivity of the LHC to these lepton-number-charged scalars. We show that, the sensitivity of high-energy colliders is largely complementary to that of low-energy and precision measurements of the decays of charged leptons, charged mesons, W and Z bosons, neutrino beam experiments like MINOS, searches for light dark matter in NA64, and searches for neutrino self-interactions at IceCube and in cosmological observations. For ϕ mass larger than a few GeV, our projected LHC sensitivity would surpass all existing bounds.

Keywords: Neutrino Non-Standard Interactions, Leptonic Scalars, Large Hadron Collider

Contents

1 Introduction

Over the past two decades, neutrino oscillations have been observed in the solar, atmospheric, reactor and accelerator neutrino experiments, revealing that at least two of the three neutrinos in the Standard Model (SM) are massive particles [1]. Yet, neutrinos remain most elusive and many questions in the neutrino sector need to be answered. Those include: (i) Are neutrinos Dirac-type or Majorana-type fermions? (ii) Is the lightest neutrino predominantly coupled to electrons in charged-current weak interactions? (iii) Is CP-invariance violated in the lepton sector? (iv) Are there non-standard interactions involving neutrinos? To answer these outstanding questions, the study of neutrino properties at all accessible experiments is strongly motivated.

If neutrinos are massive Dirac fermions, lepton-number (or some non-anomalous symmetry that contains lepton-number) is a conserved symmetry in nature. In this case, new, hypothetical particles can be characterized according to their lepton-number-charge and states associated to different lepton-number-charge will behave qualitatively differently.

For example, new scalars with lepton-number-charge equal to one only couple in pairs to SM particles and are interesting dark matter (DM) candidates [2, 3]. On the other hand, a new scalar with lepton-number-charge equal to minus two, denoted by ϕ and henceforth dubbed as a "leptonic scalar", can only couple individually to right-handed neutrinos (ν^c) like $\nu^c\nu^c\phi^*$ at the renormalizable level. At the dimension-six level, it also couples to a pair of lepton-doublets (L) and Higgs-doublets (H) like $(LH)(LH)\phi$. After electroweak (EW) symmetry breaking, the latter yields the low-energy effective Lagrangian

$$\mathcal{L} \supset \frac{1}{2}\lambda_{\alpha\beta}\, \phi\, \nu_\alpha\nu_\beta\,, \tag{1.1}$$

where α, $\beta = e$, μ, τ are the lepton-flavor indices and $\lambda_{\alpha\beta}$ the flavor-dependent Yukawa couplings. To be self-consistent, within the effective field theory (EFT) framework, we concentrate on scalar masses m_ϕ lower than the EW scale $v_{\rm EW} \simeq 246$ GeV. The couplings in Eq. (1.1) define one class of well-motivated simplified models for new neutrino self-interactions; if the momentum transfer is much smaller than the scalar mass m_ϕ, then the scalar ϕ can be integrated out and we are left with the effective four-neutrino interactions.

Given the interaction Lagrangian (1.1), the leptonic scalar ϕ can be produced by radiation off a neutrino. As such, there is a large class of processes at different energy regime to search for its existence, as we will discuss in detail. In particular, at high-energy hadron colliders, it can be produced in a unique sub-process like

$$uu \rightarrow dd\, \ell_\alpha^+\ell_\beta^+\, \phi\,, \tag{1.2}$$

where ϕ decays subsequently into neutrinos and hence manifests itself as missing energy in the vector-boson fusion (VBF) process. Generically, ϕ-production is characterized by same-sign dileptons plus two forward jets and missing transverse energy. The corresponding Feynman diagram is depicted in Fig. 1. This topology is the same as the one for the emission of a Majoron from neutrinoless double beta ($0\nu\beta\beta$) decay process [4, 5]. For Majoron masses smaller than $\mathcal{O}$(MeV) – the typical Q-value for relevant nuclei, strong limits on the coupling $\lambda_{\alpha\beta} \lesssim 10^{-4}$ have been set by $0\nu\beta\beta$ experiments like NEMO-3 [6–11], KamLAND-Zen [12], EXO-200 [13] and GERDA [14]. In this paper, we show that high-energy colliders like LHC provide a novel complementary probe of the coupling $\lambda_{\alpha\beta}$ through the VBF process (1.2) that extends the experimental reach to relatively higher ϕ masses. Note that if neutrinos were Majorana particles, one could have the lepton-number-violating process $pp \to \ell^\pm\ell^\pm jj$ at high-energy colliders, either via the VBF channel shown in Fig. 1 without the ϕ emission, or via the s-channel Keung-Senjanović process [15] involving heavy Majorana neutrinos (and heavy gauge bosons). For reviews on the current constraints and future prospects of these lepton-number-violating processes at colliders, as well as other relevant low-energy searches, including meson decays and beam dump experiments; see e.g., Refs. [16–19]. The process under consideration in Eq. (1.2) has an additional leptonic scalar ϕ that carries away missing energy and lepton-number.

In this paper, we explore the impact of the couplings $\lambda_{\alpha\beta}$, defined in Eq. (1.1), at the $\sqrt{s} = 14$ TeV LHC and the high-luminosity upgrade (HL-LHC), up to an integrated luminosity of 3 ab^{-1}, as a function of m_ϕ. We find that the LHC (HL-LHC) is sensitive to

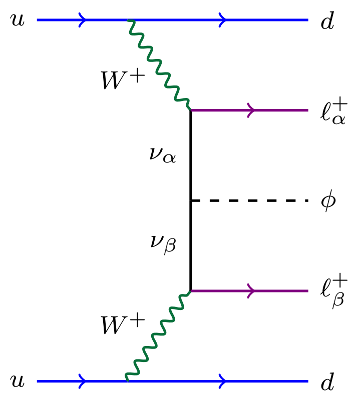

Figure 1. Representative Feynman diagram for the production of ϕ at the LHC.

couplings $\lambda_{\alpha\beta}$ as small as 1.00 (0.68) for $m_\phi \lesssim 50$ GeV. The sensitivity degrades slowly for larger m_ϕ, as the production cross section becomes smaller. The LHC prospects already exceed all the current existing limits for $m_\phi \gtrsim 1$ GeV while limits from lepton and meson decays and other low-energy data are more stringent for smaller m_ϕ [2, 20, 21]. Hence, searches for ϕ at the high-energy colliders are largely complementary to those at low-energy, high-precision setups. With higher energies and larger luminosities, the sensitivity to $\lambda_{\alpha\beta}$ is expected to be improved at the $\sqrt{s} = 27$ TeV High-Energy LHC [22] and future 100 TeV colliders like Future Circular Collider (FCC-hh) [23] and Super Proton-Proton Collider (SPPC) [24]. Studies associated to these future machines, however, go beyond the main scope of this paper and will be pursued elsewhere.

The rest of this paper is organized as follows: All the current low-energy limits on the mass m_ϕ and couplings $\lambda_{\alpha\beta}$ are collected in Section 2. Our estimates for the sensitivity at the LHC and HL-LHC to the new couplings $\lambda_{\alpha\beta}$ are given in Section 3. We present our conclusions in Section 4. Some details of the computation of the multi-body decays involving ϕ are relegated to Appendix A.

2 Low-energy Constraints

The scalar mass m_ϕ and the couplings $\lambda_{\alpha\beta}$ are constrained by a variety of high-precision data at low energy [2, 20, 21]. In this section, we focus mainly on the constraints for $m_\phi > 100$ MeV, including decay rates of tauon and charged mesons, the searches of heavy neutrinos from charged meson decays, the invisible decay width of Z boson, the production and decays of W boson at colliders, neutrino-matter scatting in neutrino beam experiments MINOS and DUNE, light DM searches in the high-intensity experiments NA64 and LDMX, and the IceCube and cosmic microwave background (CMB) limits on the new neutrino–neutrino interactions. All of these limits are collected in Table 1 and detailed in the following subsections 2.1–2.7. There are also many other limits which are relevant for a lighter ϕ with mass $m_\phi < 100$ MeV, such as those from muon decays, tritium decay, searches of Majoron in $0\nu\beta\beta$ decay experiments, supernova, relativistic degrees of freedom $\Delta N_{\rm eff}$ in the early Universe, and the neutrino decay constraints. To be complete, all of these

Table 1. Summary of current and future experimental data which can be used to set limits on the couplings $|\lambda_{\alpha\beta}|$ (with $\ell = e, \mu$) or their combinations. The last column shows the relevant m_ϕ ranges (see Figs. 2–5 and 9–11). For the limits from invisible Z decays, NA64 and LDMX, the symmetry factor $S_{\alpha\beta} = 1\,(1/2)$ for $\alpha \neq \beta$ ($\alpha = \beta$). For the IceCube data, the number in the parentheses is the future prospect. The limits not collected in this table are either weaker or not relevant for $m_\phi > 100$ MeV. The branching fraction (BR) upper limits are at 95% confidence level (C.L.), whereas the error bars quoted for the BR measurements are at 1σ C.L.; see text for more details.

Ref.	Process	Data	Couplings	Mass range
[1, 2]	$\pi^- \to e^-\bar{\nu}_e\nu\bar{\nu}$	BR $< 5 \times 10^{-6}$	$\sum_\beta |\lambda_{e\beta}|^2$	$m_\phi < 131$ MeV
[1, 2]	$K^- \to e^-\bar{\nu}_e\nu\bar{\nu}$	BR $< 6 \times 10^{-5}$	$\sum_\beta |\lambda_{e\beta}|^2$	$m_\phi < 444$ MeV
[1, 2]	$K^- \to \mu^-\bar{\nu}_\mu\nu\bar{\nu}$	BR $< 2.4 \times 10^{-6}$	$\sum_\beta |\lambda_{\mu\beta}|^2$	$m_\phi < 386$ MeV
[1, 2]	$D^- \to e^-\bar{\nu}_e$	BR $< 8.8 \times 10^{-6}$	$\sum_\beta |\lambda_{e\beta}|^2$	$m_\phi < 1.52$ GeV
[1, 2]	$D^- \to \mu^-\bar{\nu}_\mu$	BR $< 3.4 \times 10^{-5}$	$\sum_\beta |\lambda_{\mu\beta}|^2$	$m_\phi < 1.39$ GeV
[1, 21]	$D_s^- \to e^-\bar{\nu}_e$	BR $< 8.3 \times 10^{-5}$	$\sum_\beta |\lambda_{e\beta}|^2$	$m_\phi < 1.64$ GeV
[1, 21]	$D_s^- \to \mu^-\bar{\nu}_\mu$	BR $= (5.50 \pm 0.23) \times 10^{-3}$	$\sum_\beta |\lambda_{\mu\beta}|^2$	$m_\phi < 1.50$ GeV
[1, 21]	$B^- \to e^-\bar{\nu}_e$	BR $< 9.8 \times 10^{-7}$	$\sum_\beta |\lambda_{e\beta}|^2$	$m_\phi < 3.54$ GeV
[1, 21]	$B^- \to \mu^-\bar{\nu}_\mu$	BR $= (2.90 - 10.7) \times 10^{-7}$	$\sum_\beta |\lambda_{\mu\beta}|^2$	$m_\phi < 3.50$ GeV
[1, 20]	$\tau^- \to e^-\bar{\nu}_e\nu_\tau$	BR $= (17.82 \pm 0.04)\%$	$\sum_\beta |\lambda_{e\beta}|^2$	$m_\phi < 741$ MeV
[1, 20]	$\tau^- \to \mu^-\bar{\nu}_\mu\nu_\tau$	BR $= (17.39 \pm 0.04)\%$	$\sum_\beta |\lambda_{\mu\beta}|^2$	$m_\phi < 741$ MeV
[1, 21]	$P^- \to e^- N$	see Ref. [25]	$\sum_\beta |\lambda_{e\beta}|^2$	$3.3\,\text{MeV} < m_\phi < 448$ MeV
[1, 21]	$P^- \to \mu^- N$	see Ref. [25]	$\sum_\beta |\lambda_{\mu\beta}|^2$	$87\,\text{MeV} < m_\phi < 379$ MeV
[1]	$Z \to$ inv.	BR $= (20.0 \pm 0.055)\%$	$\sum_{\alpha,\beta} S_{\alpha\beta}|\lambda_{\alpha\beta}|^2$	$m_\phi < 52.2$ GeV
[1]	$W \to e\nu$	BR $= (10.71 \pm 0.16)\%$	$\sum_\beta |\lambda_{e\beta}|^2$	$m_\phi < 38.8$ GeV
[1]	$W \to \mu\nu$	BR $= (10.63 \pm 0.15)\%$	$\sum_\beta |\lambda_{\mu\beta}|^2$	$m_\phi < 39.3$ GeV
[2]	MINOS	see Ref. [2]	$|\lambda_{\mu\mu}|$	$m_\phi < 1.67$ GeV
[2]	DUNE	see Ref. [2]	$|\lambda_{\mu\mu}|$	$m_\phi < 3.00$ GeV
[26]	NA64	see Ref. [26]	$\sum_{\alpha,\beta} S_{\alpha\beta}|\lambda_{\alpha\beta}|^2$	$m_\phi < 948$ MeV
[27]	LDMX	see Ref. [27]	$\sum_{\alpha,\beta} S_{\alpha\beta}|\lambda_{\alpha\beta}|^2$	$m_\phi < 1.50$ GeV
[28, 29]	IceCube	see Ref. [28]	$|\lambda_{\alpha\beta}|$	$m_\phi < 2.0\,(15.0)$ GeV

are summarized in Section 2.8, but not used in our analysis, mainly because the new LHC sensitivities derived here become competitive only in the high-mass regime with $m_\phi \gtrsim 100$ MeV. In Section 3, we focus only on the LHC prospects for the couplings $\lambda_{ee,\,e\mu,\,\mu\mu}$ that do not involve the τ-lepton flavor in the final state shown in Fig. 1, therefore we exclude the couplings $\lambda_{\alpha\beta}$ involving the τ flavor from Table 1 and Figs. 2–5. For completeness, we will comment on the limits on τ-flavor relevant couplings in the text, when they are applicable.

2.1 Meson decay rates

For leptonic decays of charged mesons $P^- \to \ell^-\bar{\nu}$ with $P^- = \pi^-, K^-, D^-, D_S^-, B^-$, the leptonic scalar ϕ can be emitted from the neutrino line in the final state and this process is not suppressed by the helicity of the charged lepton, with the partial width [21]

$$\Gamma(P^- \to \ell_\alpha^-\bar{\nu}\phi) = \frac{G_F^2|V_{qq'}|^2 m_P^3 f_P^2 \sum_\beta |\lambda_{\alpha\beta}|^2}{256\pi^3} \times \int_{x_\phi}^{(1-\sqrt{x_\ell})^2} \mathrm{d}x \frac{\left((x+x_\ell)-(x-x_\ell)^2\right)(x-x_\phi)^2}{x^3} \lambda^{1/2}(1,\,x,\,x_\ell)\,, \quad (2.1)$$

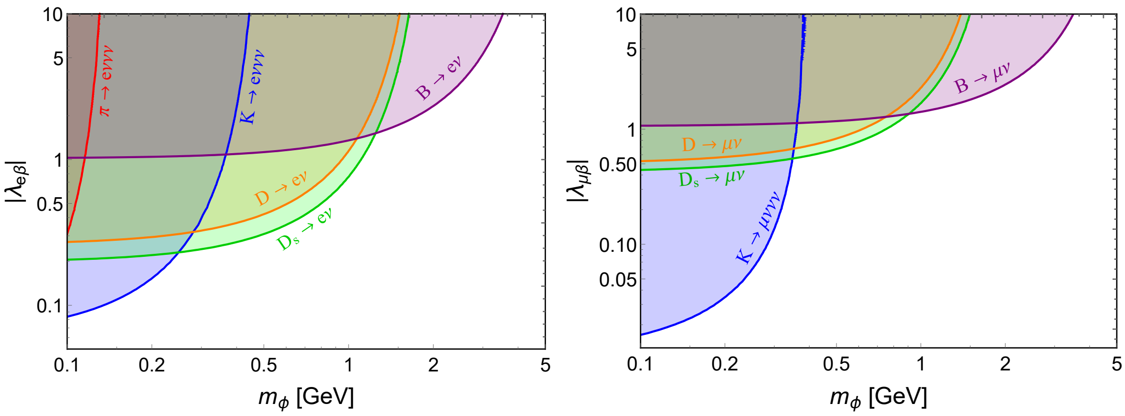

Figure 2. Limits on $|\lambda_{e\beta}|$ (left panel) and $|\lambda_{\mu\beta}|$ (right panel) with $\beta = e,\, \mu,\, \tau$ from current-charged meson decay data in Table 1. All the shaded regions are excluded.

where $\lambda(a,\, b,\, c) \equiv a^2 + b^2 + c^2 - 2ab - 2ac - 2bc$, $V_{qq'}$ are the CKM matrix elements with the valence quarks q and q' for the meson, m_P and f_P are respectively the meson mass and decay constant, $x_{\ell,\,\phi} \equiv m^2_{\ell,\,\phi}/m_P$, with m_ℓ the charged lepton mass, the charged lepton flavor $\alpha = e,\, \mu$ and we have summed over the neutrino flavor $\beta = e,\, \mu,\, \tau$ in the final state. For the light mesons $\pi^\pm$ and $K^\pm$, the rare decays $\pi^-,\, K^- \to e^-\nu_e\nu\bar{\nu}$ and $K^- \to \mu^-\nu_\mu\nu\bar{\nu}$ have been searched for in experiments [30–32], and the upper limits on the branching fractions are collected in Table 1. These processes correspond to the decays $\pi^-,\, K^- \to \ell^-\bar{\nu}\phi$ with $\phi \to \nu\nu$, and the experimental data can be used to set limits on the couplings $\sum_\beta |\lambda_{e\beta}|^2$ and $\sum_\beta |\lambda_{\mu\beta}|^2$. For simplicity, we assume only one of the couplings $\lambda_{\alpha\beta}$ to be non-vanishing while deriving the limits. The results for $|\lambda_{e\beta}|$ and $|\lambda_{\mu\beta}|$ are shown respectively in the left and right panels of Fig. 2. For the heavier mesons $D^\pm$, $D_s^\pm$ and $B^\pm$, we adopt the experimental upper limits on the BRs at the 95% C.L. in Table 1 [1] to set limits on the couplings $|\lambda_{\alpha\beta}|$, as shown in Fig. 2. For the measurements with 1σ error bars in Table 1, we also obtain the 95% C.L. limits on the $\lambda_{\alpha\beta}$ couplings by simply multiplying the error bars by a factor of 1.96. There are also some limits on the meson decays to tauon leptons [1]; however, these limits are too weak to impose any constraints on the couplings $\lambda_{\tau\beta}$.

2.2 Heavy neutrino searches in meson decay spectra

Heavy neutrinos N have been searched for in two-body meson decays, such as $\pi^- \to e^-N$ and $K^- \to \ell^-N$ (with $\ell = e,\, \mu$) by several experiments, including TRIUMF [33], PIENU [34], KEK [35], E949 [36], OKA [37] and NA62 [25, 38]. The peak searches in the lepton energy spectrum can be used to set limits on the leptonic scalar couplings to neutrinos, by comparing the lepton spectra of the two-body decays $P^- \to \ell^-N$ to those of the three-body decays $P^- \to \ell\nu\phi$ [21]. For the two-body decays of charged mesons, the differential partial width with respect to the charged lepton momentum p_ℓ is given by [21]

$$\frac{\mathrm{d}}{\mathrm{d}p_\ell}\Gamma(P^- \to \ell^-N) \;\simeq\; \rho\Gamma_0(P^- \to \ell^-\bar{\nu})|U_{\ell N}|^2\delta(p_{\rm peak} - p_\ell) \tag{2.2}$$

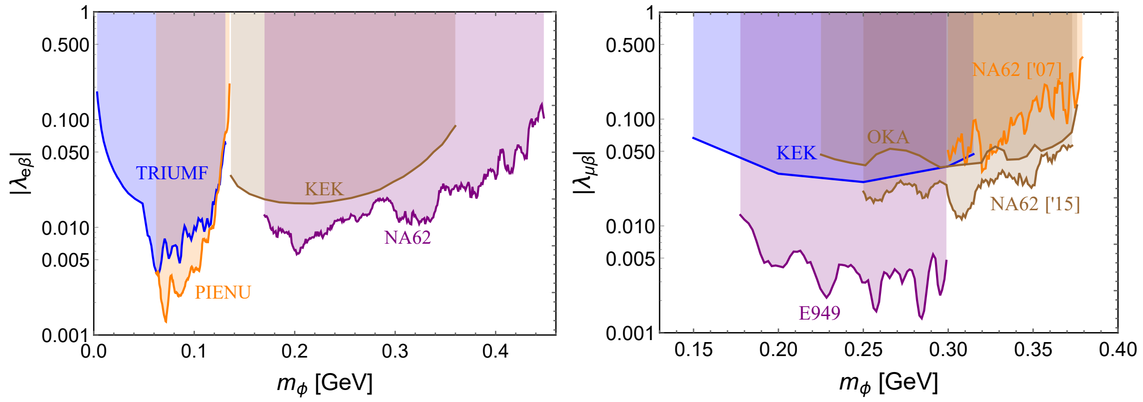

Figure 3. Limits on $|\lambda_{e\beta}|$ (left panel) and $|\lambda_{\mu\beta}|$ (right panel) with $\beta = e,\, \mu,\, \tau$ from heavy neutrino searches in meson decays in TRIUMF [33], PIENU [34], KEK [35], E949 [36], OKA [37], NA62 ['07] [38] and NA62 ['15] [25]. The shaded regions are excluded.

with $\Gamma_0(P^- \to \ell^- \nu)$ the leading order (LO) leptonic meson decay width in the SM:

$$\Gamma_0(P^- \to \ell_\alpha^- \bar{\nu}) \;=\; \frac{G_F^2 |V_{qq'}|^2 m_P^3 f_P^2}{8\pi} x_\ell (1 - x_\ell)^2 \,, \tag{2.3}$$

$|U_{\ell N}|$ is the heavy-light neutrino mixing angle, and

$$\rho \;=\; \frac{x_\ell + x_N - (x_\ell - p x_N)^2}{x_\ell (1 - x_\ell)^2} \lambda^{1/2}(1,\, x_\ell,\, x_N) \,, \tag{2.4}$$

where we have defined $x_N \equiv m_N^2/m_P^2$ with m_N being the heavy neutrino mass. For the three-body decays, on the other hand,

$$\begin{aligned} \frac{\mathrm{d}}{\mathrm{d}p_\ell}\Gamma(P^- \to \ell_\alpha^- \nu \phi) \;&=\; \frac{G_F^2 |V_{qq'}|^2 m_P^3 f_P^2 |\lambda_{\alpha\beta}|^2}{128\pi^3} \left[(x + x_\ell) - (x - x_\ell)^2 \right] \\ &\quad \times \frac{(x - x_\phi)^2}{x^3 \sqrt{x_\ell^2 + p_\ell^2/m_P^2}} \frac{p_\ell}{m_P^2} \lambda^{1/2}(1, x, x_\ell) \,, \end{aligned} \tag{2.5}$$

where $x \equiv 1 + x_\ell - 2\sqrt{x_\ell + p_\ell^2/m_P^2}$. By setting m_ϕ equal to m_N, and demanding that the lepton energy spectrum in the three-body case should not exceed the observed spectrum for the two-body case at any value of energy, the resultant limits on the couplings $|\lambda_{e\beta}|$ and $|\lambda_{\mu\beta}|$ are collected respectively in the left and right panels of Fig. 3. As the constraints on heavy-light neutrino mixing angle $|U_{\ell N}|$ are very stringent, the limits on $|\lambda_{\alpha\beta}|$ from the meson decay spectra are very strong, down to $\sim 10^{-3}$.

In addition to the two-body decays of meson, heavy neutrino can also be searched for by (partially) reconstructing the decay products of heavy neutrino, for instance, in the decay chain $B \to X \ell N$, $N \to \ell\pi$, $\ell_\alpha^+ \ell_\beta^- \nu$ with X being any SM particle. Such direct searches have been performed in the experiments PS191 [39, 40], BEBC [41], NA3 [42], NuTeV [43], LHCb [44–46], Belle [47], NA48/2 [48] and T2K [49], and also proposed in future experiments like FASER [50, 51], MATHUSLA [52, 53], CODEX-b [54, 55], AL3X [56],

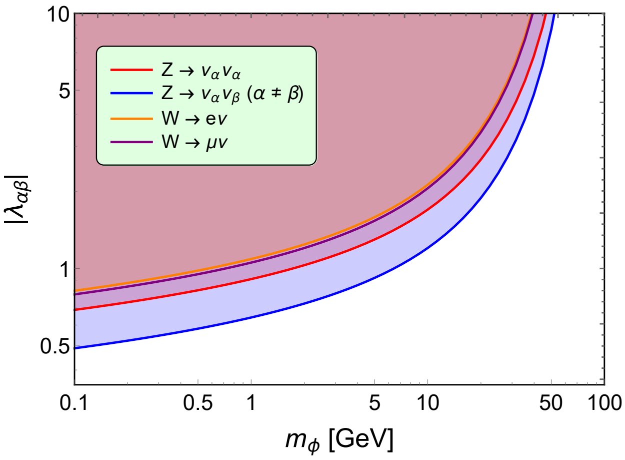

Figure 4. Limits on $|\lambda_{\alpha\beta}|$ (with α, $\beta = e$, μ) from W and Z decay data in Table 1. The shaded regions are excluded.

SHiP [57, 58] and DUNE [59]. Although the heavy-light neutrino mixing angles $|U_{\ell N}|$ are (or can be) tightly constrained by these experimental data, these limits from N decay products can not be used directly to set limits on the couplings $\lambda_{\alpha\beta}$ in our case, as the ϕ decays to invisible neutrinos; therefore, we do not consider these limits here.

2.3 W and Z decay rates

The leptonic scalar ϕ could couple to the neutrinos coming from Z decays and thus induce extra contribution to invisible decay width of the Z boson. The analytical calculations of $\Gamma(Z \to \nu_\alpha \nu_\beta \phi)$ are presented in Appendix A.1. The combined LEP result for the BR of invisible Z decays is $\text{BR}(Z \to \text{inv.}) = (20.0 \pm 0.055)\%$ [60–63]. The resultant constraints on the couplings $\lambda_{\alpha\beta}$ at 2σ C.L. are shown in Fig. 4. The red and blue shaded regions are respectively for the couplings $|\lambda_{\alpha\alpha}|$ and $|\lambda_{\alpha\beta}|$ (with $\alpha \neq \beta$). Note that Ref. [2] also considered the Higgs boson invisible decay width constraints (arising from an additional $\nu\nu\phi h$ term in the Lagrangian), which were comparable to or even stronger than the Z decay constraints. However, with the minimal interaction term in Eq. (1.1), we do not have any such exotic Higgs decay modes that could give comparable constraints.

In an analogous way, the leptonic scalar ϕ can also be emitted in the decays of $W \to \ell\nu$ with $\ell = e, \mu, \tau$. Therefore, the couplings $\lambda_{\alpha\beta}$ can be constrained by leptonic W decay rates using the analytical expression given in Appendix A.1 [cf. Eq. (A.6)]. The current LEP uncertainties for the e, μ and τ flavor leptonic W decays are respectively 0.16%, 0.15% and 0.21% at 1σ C.L. [64–67]. The corresponding limits on $|\lambda_{\alpha\beta}|$ at 2σ C.L. are shown in Fig. 4. The orange and purple lines are respectively for the e and μ flavors. In addition, we also have the limits from the following W-related final states at LEP and LHC, which however turn out to be much weaker and are not shown in Fig. 4:

- The W production cross section times branching fraction for the Drell-Yan process $pp \to W \to \ell\nu$ has been measured at the LHC. The distributions of the transverse momentum p_T of charged lepton, missing energy and the transverse mass of W boson have also been measured by both ATLAS [68–72] and CMS [73–78]. For sufficiently large couplings $\lambda_{\alpha\beta}$, the leptonic scalar ϕ can be produced from $W \to \ell\nu\phi$ and potentially modify the distributions above, which can in principle be used to set limits on scalar mass m_ϕ and the couplings $\lambda_{\alpha\beta}$. However, even if we use the current most precise data from Ref. [72], the experimental uncertainties are still too large, of order 0.5%, when compared to, e.g., those from Z decay (at the level of 0.05%), and therefore, we cannot obtain stronger constraints from these distributions.

- The charged lepton energy distribution has also been measured in the W-pair production process $e^+e^- \to W^+W^- \to q\bar{q}\ell\nu$ at LEP [64]. In principle, these distributions can be used to set limits on the couplings $\lambda_{\alpha\beta}$. However, the experimental uncertainties again turn out to be too large to put any stronger constraints than those obtained from W and Z decay.

- The electron-muon universality has also been tested in the W decay at LHC [71]. However, the current experimental uncertainties are at 1% level, and therefore, the universality constraints are expected to much weaker than those from the W and Z decay rates.

- One can also use other LHC data involving W boson to estimate the constraints on $\lambda_{\alpha\beta}$, such as the top quark pair-production at LHC. However, the inclusive cross section for $pp \to t\bar{t}$ is at least four times smaller than that for single W production at LHC [79], and the SM backgrounds for top quark events are more complicated. Therefore we expect the limits from $t \to Wb \to \ell\nu b$ should be significantly weaker than those from W data itself.

2.4 Tauon decay rates

If kinematically allowed, the leptonic scalar ϕ could also be produced from lepton decays, such as $\mu \to e\nu\nu\phi$ and $\tau \to \ell_\alpha\nu\nu\phi$ (with $\alpha = e,\, \mu$). In the limit of $m_\phi \to 0$ (or $m_\phi \ll m_\mu$) the μ decay limits are expected to be much stronger than those from τ decays [20], because the Michel electron spectrum from muon decay has been measured very precisely [1]. However, when the scalar mass $m_\phi \gtrsim 100$ MeV the decay $\mu \to e\nu\nu\phi$ is either kinematically forbidden or highly suppressed, and therefore, we only consider the tauon decays in this subsection. The calculation of partial width for the four-body decays $\Gamma(\tau \to \ell_\alpha\nu\nu\phi)$ is outlined in Appendix A.2. The partial widths $\Gamma(\tau \to e\nu\nu\phi)$ and $\Gamma(\tau \to \mu\nu\nu\phi)$ are compared to the experimental uncertainties for the leptonic decays $\mathrm{BR}(\tau \to e\nu\nu)$ and $\mathrm{BR}(\tau \to \mu\nu\nu)$, which turn out to be 4×10^{-4} at the 1σ level for both e and μ [1]. As the leptonic scalar ϕ can be emitted from the ν_α and/or ν_τ fermion lines, all the flavor combinations of $\lambda_{\alpha\beta}$ get constrained by the τ decay data, including $\lambda_{\tau\tau}$ which is barely constrained by meson decays. It turns out that the tauon decay limits on all flavor combinations $\lambda_{\alpha\beta}$ are roughly the same, as summarized in Figs. 9–11. For a scalar mass of $m_\phi = 100$ MeV, it is required that $|\lambda_{\alpha\beta}| \lesssim \mathcal{O}(1)$. The constraints in the $m_\phi \to 0$ limit are $|\lambda_{\alpha\beta}| \lesssim 0.3$, which is consistent with the numbers given in Ref. [20].

2.5 Neutrino beam experiments

As stated in Ref. [2], the light leptonic scalar ϕ can be emitted from neutrino beams via neutrino-matter scattering such as $\nu_\alpha + p \to \ell_\beta^+ + n + \phi$ (where p and n stand for proton and neutron, respectively). This will affect the charged lepton momentum distributions in the final state, and more importantly, the charged lepton in this process seems to have the wrong sign due to the emission of lepton-number-charged ϕ. The magnetized MINOS detector can distinguish the charges of $\mu^\pm$ produced from charge-current neutrino-nucleon interactions [80], and as a consequence, the coupling $|\lambda_{\mu\mu}|$ is constrained to be smaller than $\mathcal{O}(1)$ for a 100 MeV scalar mass, as shown by the green shaded region in Fig. 11. With more charged-current events collected at DUNE [59], the coupling $|\lambda_{\mu\mu}|$ could be probed to a smaller value. For instance, assuming the most aggressive cut of no missing transverse momentum [2], the prospects of $|\lambda_{\mu\mu}|$ are expected to be enhanced by one order of magnitude, as shown by the dashed green line in Fig. 11. The MiniBooNE limit on $|\lambda_{e\mu}|$ is also considered in Ref. [2], which turns to be weaker than those shown in Fig. 10.

The NOMAD experiment searched for neutrino oscillation in $\nu_\mu \to \nu_\tau$ channel [81], but no charged-current ν_τ event was found, and a limit was imposed on the $\nu_\mu - \nu_\tau$ oscillation probability, which can be translated to a limit on the leptonic scalar mass m_ϕ and coupling $|\lambda_{\mu\tau}|$ [2]. The tauon events are difficult to be identified in the DUNE near detector, thus the DUNE prospect of $|\lambda_{\mu\tau}|$ is expected to be weaker than that from NOMAD. Similarly, the limit on the $\nu_e - \nu_\tau$ oscillation probability is weaker than that for $\nu_\mu \to \nu_\tau$.

2.6 Light dark matter searches in high-intensity experiments

As the leptonic scalar ϕ decays invisibly into light neutrinos, it can be constrained by the searches of light DM χ in the high-intensity experiments. For instance, the dark photon A' has been searched for in the NA64 experiment [26] via the electron-nuclei scattering process, with A' subsequently decaying into a pair of DM particles:

$$e\mathcal{N} \;\to\; e\mathcal{N}A', \quad A' \;\to\; \chi\chi\,, \tag{2.6}$$

with $\mathcal{N}$ being the incident nuclei. The presence of ϕ in our case would induce the process

$$e\mathcal{N} \;\to\; e\mathcal{N}\nu\nu + \phi\,, \tag{2.7}$$

via the fusion of two Z bosons, similar to that shown in Fig. 1 (with the W bosons and charged leptons replaced respectively by Z and neutrinos). The final states are the same as that for the DM searches, i.e. the scattered nuclei and electron plus significant missing energy. Therefore the limits on the DM mass $m_{A'}$ and the kinetic mixing ε of dark photon with the SM photon from the NA64 experiment can be recast into limits on the $\lambda_{\alpha\beta}$ coupling and mass m_ϕ in our case.

For the DM process in Eq. (2.6), the dark photon A' can be emitted from any of the charged fermion lines, and the cross section is proportional to

$$\sigma_{A'} \;\propto\; 3\int \mathrm{d}\Phi_3 (e\varepsilon)^2\,, \tag{2.8}$$

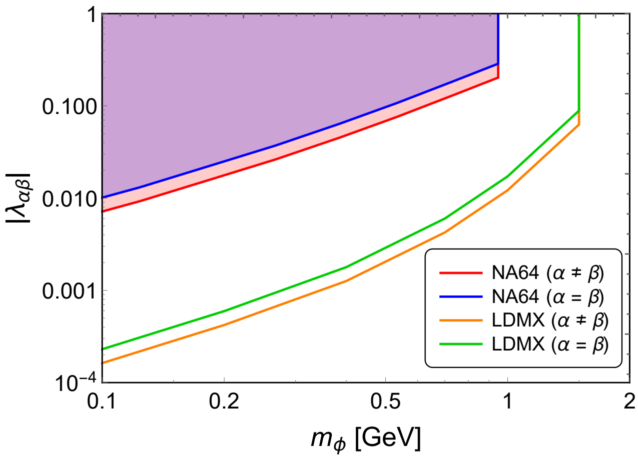

Figure 5. Limits on $|\lambda_{\alpha\beta}|$ from light DM searches in NA64 [26], and the prospects at LDMX [27]. The shaded regions are excluded.

with $d\Phi_n$ the n-body phase space, e the electromagnetic coupling constant and the prefactor 3 accounting for the three degrees of freedom of dark photon. For the ϕ-induced $2 \to 5$ process in Eq. (2.7), the production cross section is proportional to

$$\sigma_\phi \propto \int d\Phi_5 S_{\alpha\beta} |\lambda_{\alpha\beta}|^2 \,, \tag{2.9}$$

with $S_{\alpha\beta} = 1$ (1/2) the symmetry factor for $\alpha \neq \beta$ ($\alpha = \beta$). Setting the ϕ mass to be the same as $m_{A'}$, we can compare the cross sections of the two processes in Eqs. (2.8) and (2.9). The NA64 limits on $|\lambda_{\alpha\beta}|$ are expected to be roughly $\sqrt{3}(4\pi^2)e\, S_{\alpha\beta}^{-1} \simeq 20\, S_{\alpha\beta}^{-1}$ times weaker than the original NA64 limit on ε for the dark photon case, with the factor of $4\pi^2$ from comparing the phase space factors of $d\Phi_3$ and $d\Phi_5$. The resultant NA64 limits on the couplings $|\lambda_{\alpha\beta}|$ are shown in Fig. 5, with the shaded red and blue regions excluded respectively for $|\lambda_{\alpha\beta}|$ ($\alpha \neq \beta$) and $|\lambda_{\alpha\alpha}|$. With a higher luminosity, the limits can be improved by almost two orders of magnitude at LDMX [27]. The expected sensitivities of $|\lambda_{\alpha\beta}|$ ($\alpha \neq \beta$) and $|\lambda_{\alpha\alpha}|$ are shown in Fig. 5 respectively by the orange and green lines.

The process $e\mathcal{N} \to e\mathcal{N}A'$ has also been searched for in the DarkLight experiment for a lighter dark photon with mass $m_{A'} < 100$ MeV [82], and the corresponding limits on $|\lambda_{\alpha\beta}|$ are not included in Fig. 5. The searches of dark photon in the process $e^+e^- \to \gamma + A'$ with $A' \to$ inv. has been performed in the BaBar experiment [83], and also proposed in VEPP-3 [84, 85]. The final state in this case is a mono-energetic photon plus missing energy. The ϕ can not induce such signals in our case, so these limits can not be used on the $\lambda_{\alpha\beta}$ couplings.

2.7 Astrophysical and cosmological limits on neutrino self-interactions

A few PeV neutrino events have been observed in the IceCube neutrino experiment [86–88]. These high-energy neutrinos could in principle induce neutrino–neutrino interactions in the early universe, such as the ones mediated by a scalar field ϕ [28, 29, 89] as in our case. For scalar mass $m_\phi \gtrsim 100$ MeV, the ϕ mediated neutrino–neutrino interactions are practically effective four-neutrino interactions. Thus the IceCube PeV neutrino limits on neutrino–neutrino interactions can be translated to a constraint on $|\lambda_{\alpha\beta}|^2/m_\phi^2$ as shown by the shaded blue region in Figs. 9–11 which are universal for all the three neutrino flavors. Future IceCube data will improve the limits significantly [28, 29], as shown by the dashed blue line in Figs. 9–11.

The ϕ-mediated self-interactions of neutrinos also have some effects in the early Universe. In particular, neutrino free streaming will alter the CMB temperature power spectrum [90–92]. Current precision cosmological data have excluded the effective coupling $G_{\rm eff} \simeq |\lambda_{\alpha\beta}|^2/m_\phi^2 \gtrsim 2.5 \times 10^7 G_F$ [92–97]. This constraint is however weaker than the IceCube constraints discussed above, and hence, not shown in Figs. 9–11.

2.8 Other limits

When the leptonic scalar ϕ is light, with $m_\phi \lesssim 100$ MeV, its couplings to neutrinos could also induce very rich phenomena, some of which lead to very stringent limits on $\lambda_{\alpha\beta}$. For such light scalars the prospects of the couplings $\lambda_{\alpha\beta}$ at LHC and HL-LHC are almost independent of m_ϕ, as can be seen in Figs. 9–11 (see Section 3.3) and cannot compete with the low energy processes. Therefore, we restrict the ϕ mass to 100 MeV and do not show these low-energy limits in Figs. 2–5 and 9–11. Nevertheless, for completeness, we list some of these processes below:

- *Muon decay*: As discussed in Section 2.4, ϕ can be emitted from tree-level decay $\mu \to e\nu\nu\phi$. As a result of the precise μ decay data, for sufficiently light ϕ, the limits from μ decay are expected to be much more stringent than those from τ decays. In addition, the electron [98, 99] and neutrino [100, 101] spectra could be altered in presence of ϕ, which can also be used to set limits on $\lambda_{\alpha\beta}$.

- *Tritium decay*: If the scalar mass $m_\phi \lesssim \mathcal{O}(10\,\text{eV})$, it can be produced from tritium decay in the process $^3\text{H} \to {}^3\text{He}^+ + e^- + \nu + \phi$ [102], and this process can be probed in the KATRIN experiment [103, 104].

- $0\nu\beta\beta$ *decay*: The coupling of ϕ to electron neutrinos contributes to $0\nu\beta\beta$ decays via the process $(Z, A) \to (Z+2, A)e^-e^-\phi$ if the mass $m_\phi \lesssim \mathcal{O}(\text{MeV})$ – the typical Q-value for the relevant nuclei. This is strongly constrained by the searches of Majoron emission in $0\nu\beta\beta$ decay experiments like NEMO-3 using ^{100}Mo [6, 7, 11] and ^{150}Nd [9] nuclei, as well as KamLAND-Zen [12] and EXO-200 [13] using ^{136}Xe. Somewhat weaker limits were also obtained by NEMO-3 using ^{48}Ca [8] and ^{82}Se [10], as well as by GERDA using ^{76}Ge [14].

- *Supernovae*: A light ϕ can be produced abundantly in the supernova core if its mass $m_\phi \lesssim \mathcal{O}(30\,\text{MeV})$ – the typical core temperature of supernovae. The couplings $|\lambda_{\alpha\beta}|$ can be constrained from both the luminosity and deleptonization arguments [105–107].

- *CMB and BBN*: As a light particle, ϕ itself contributes to the relativistic degrees of freedom $N_{\rm eff}$ if the mass $m_\phi \lesssim 100$ keV [108]. The current precision cosmological data

$\Delta N_{\rm eff} = 0.18$ at 1σ C.L. [109] has excluded a large parameter space for such light leptonic scalar mass m_ϕ and the couplings $|\lambda_{\alpha\beta}|$. Similarly, the big-bang-nucleosynthesis (BBN) constraints rule out $m_\phi \lesssim 0.2$ MeV for sizable couplings $\lambda_{\alpha\beta}$, as long as they allow ϕ particles to thermalize at BBN temperature [110].

- *Neutrino decay*: For sufficiently light ϕ, the heavier neutrinos might decay via $\nu_j \to \nu_i + \phi$ with the mass indices $i, j = 1, 2, 3$ and $i < j$. Therefore we can impose stringent bounds on the leptonic scalar mass m_ϕ and the λ_{ij} couplings from the solar neutrino data [111–115]. There are also constraints from atmospheric and long baseline experiments [116–118]. The CMB limits on neutrino free streaming could also set limits on neutrino decays, as long as the mediator is lighter than neutrino mass and the non-diagonal couplings λ_{ij} are non-vanishing [93, 94, 119].

3 Prospects at the LHC and HL-LHC

At high-energy colliders, W and Z boson decays can give rise to the leptonic scalar ϕ via its couplings to neutrinos if kinematically allowed ($m_\phi < M_W$), as discussed in Section 2.3. Instead, in this section, we explore the direct production of ϕ at the LHC that could potentially extend the reach to higher masses. At the leading order, ϕ can be produced in the VBF processes $W^\pm W^\pm \to \ell^\pm \ell^\pm \phi$, leading to the unique signal of same-sign dileptons at hadron colliders:

$$pp \;\to\; \ell^\pm_\alpha \ell^\pm_\beta \; \phi \; jj \,, \tag{3.1}$$

where $\alpha, \beta = e, \mu$ are the flavor indices. In a VBF process, two incoming quarks can emit virtual same-sign W bosons, which then interact to produce a pair of same-sign leptons via t/u-channel neutrino exchange. The leptonic scalar ϕ is irradiated by the t/u-channel neutrino. A representative diagram of the process is shown in Fig. 1. The advantage of VBF processes is that the energy available in the same-sign W-pair system peaks at $\sim 2M_W$, and most of this energy is carried by the same-sign leptons. Consequently, the production cross section of the $\ell^\pm \ell^\pm \; \phi \; jj$ process is not sensitive to a large range of m_ϕ. In Fig. 6, we show the variation of the production cross section of the above process (3.1) at the $\sqrt{s} = 14$ TeV LHC as a function of m_ϕ in solid red. In a broad range of mass, the cross section is of $\mathcal{O}(1 \text{ fb})$. It is evident from Fig. 6 that the creation of ϕ at the LHC via VBF processes starts feeling the effect of ϕ mass only for $m_\phi \gtrsim 10$ GeV. For comparison, we also show the cross section curve of the process for a 100 TeV pp collider in dashed blue. The production rate will be increased by about a factor of 20.

We only consider $\ell = e, \mu$ in the present study for simplicity. We will comment on the impact of including signals from leptonic τ decays for our results. However, including hadronic τ decays in the analysis will require careful examination of a different set of SM backgrounds dominated by τ_h charge misreconstruction processes, which we postpone for a future study.

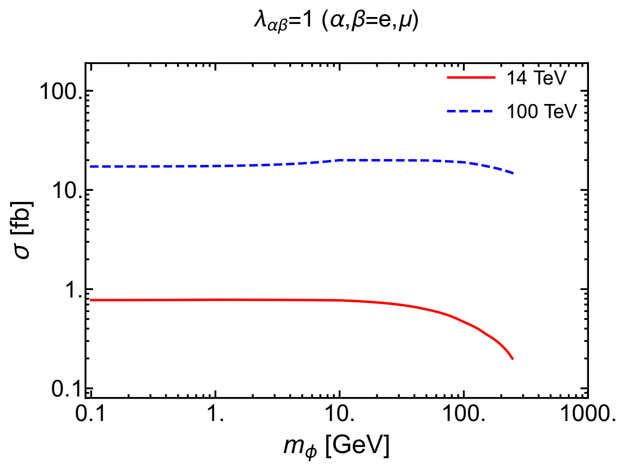

Figure 6. Production cross section of the $pp \to \ell_\alpha^\pm \ell_\beta^\pm\ \phi\ jj$ process at $\sqrt{s} = 14$ TeV and 100 TeV, as a function of the mass of ϕ, with the Yukawa couplings $\lambda_{\alpha\beta} = 1$ (α, $\beta = e$, μ). For different coupling values, the corresponding cross sections can be obtained from the scaling $\sigma \propto |\lambda_{\alpha\beta}|^2$. We stop at $m_\phi = v_{\rm EW}$ beyond which the EFT approach used to define the effective $\nu\nu\phi$ coupling in Eq. (1.1) may not be reliable.

3.1 SM backgrounds and simulation details

Our strategy to search for ϕ is based on two steps. First, we use the distinct features of VBF processes to reduce non-VBF QCD backgrounds. A VBF process is characterized by two back-to-back energetic jets in the forward/backward region of the detector, with large di-jet invariant mass, and significant separation in rapidity $|\Delta y_{j_1 j_2}|$. To select the VBF topology we roughly follow the strategy used in a recent ATLAS $W^\pm W^\pm jj$ analysis [120]. Finally, we impose stringent cuts on the transverse momentum of the leptons, and the azimuthal separation between the leading lepton and transverse missing energy ($E_T^{\rm miss}$) to suppress the irreducible EW $W^\pm W^\pm jj$ background.

The dominant SM background processes for our chosen final state are

- the EW process $pp \to W^\pm W^\pm jj \to jj\ell_\alpha^\pm \ell_\beta^\pm \nu\nu$,
- the QCD process $pp \to W^\pm W^\pm jj \to jj\ell_\alpha^\pm \ell_\beta^\pm \nu\nu$,
- $pp \to W^\pm Zjj \to jj\ell_\alpha^\pm \ell_\beta^\pm \ell_\beta^\mp \nu$,

with the lepton flavor indices α, $\beta = e$, μ, τ. One should note that although we do not consider light leptons coming from τ decays for the signal, we do include them for backgrounds. The $W^\pm Zjj$ background is generated inclusively and consists of both QCD and EW processes. Both the EW and QCD $W^\pm W^\pm jj$ processes have the same final state as the ϕ-induced signal, i.e., a pair of same-sign dilepton, two hard jets and large $E_T^{\rm miss}$. At the leading order, the EW $W^\pm W^\pm jj$ background is dominated by the vector-boson scattering $W^\pm W^\pm \to W^\pm W^\pm$, mediated by a t-channel Z/γ, which has recently been observed by both ATLAS [120] and CMS [121]. On the other hand, the QCD $W^\pm W^\pm jj$ background is mediated by a t-channel gluon. As we will see soon, the QCD $W^\pm W^\pm jj$ background is effectively suppressed by the VBF cuts. For the $W^{\pm}Zjj$ background, one of the charged leptons coming from the Z decay is missed by the detectors, and we are left with only two isolated leptons in the final state.

There are also some sub-leading backgrounds, such as the charged leptons from heavy-flavor hadron decays, jets misidentified as leptons, backgrounds coming from lepton charge misidentification and the $V\gamma$ production with photon misidentified as electron [120, 121]. However, all these backgrounds are due to detector effects and are impossible to simulate reliably within our simulation setting. So, we will not consider the above backgrounds in our analysis. However, they can contribute at 20% level after the VBF cuts [120]. We expect that the hard lepton p_T and $|\Delta\phi_{\ell_1,E_T^{\rm miss}}|$ cuts will suppress them significantly due to their efficiency in removing the dominant SM backgrounds (see Table 2). In addition, other non-prompt backgrounds like ZZ, VVV and $t\bar{t}V$ ($V = W, Z$) contribute $< 2\%$ to the total background after the VBF cuts [120], and are not considered here.

We simulate the signal and background events by using `MadGraph5_v2_5_4` [122] with the `NNPDF2.3` LO parton distribution functions [123]. We pass the simulated events to `Pythia8` [124] for showering and hadronization, and subsequently to `Delphes-3.4.1` [125] for detector simulation. The $W^{\pm}, Z$ bosons in SM backgrounds and the scalar ϕ in the signal are decayed to leptons and neutrinos by using the `Madspin` [126] module of `MadGraph5`.

In our detector simulation with `Delphes`, electrons and muons are identified with $p_T > 10$ GeV and $|\eta| \leq 2.5$. While the muon efficiency is 95% for the entire range of $|\eta|$, the electron efficiency is 95% (85%) for $|\eta| \leq 1.5$ ($1.5 < |\eta| \leq 2.5$). The lepton isolation is parameterized by $I_{\rm rel} < 0.12\,(0.25)$ for electron (muon), where $I_{\rm rel}$ is the ratio of the p_T sum of objects (tracks, calorimeter towers, etc) within a $\Delta R = \sqrt{(\Delta\eta)^2 + (\Delta\phi)^2} = 0.4$ cone around a candidate, and the candidate's p_T. Jets are clustered using the anti-k_T algorithm [127] with cone radius 0.5 and $p_T > 20$ GeV. We use the default b-tagging algorithm of `Delphes` where the b-tagging efficiency is just above 70% for transverse momenta between 85 and 250 GeV, with a mistag rate $\lesssim 2\%\,(20\%)$, coming from light jets, i.e. from gluon and up, down, strange (and charm) quarks, over the same p_T range.

We perform a calibration study to check the lepton isolation performance of `Delphes` against the $\ell^{\pm}\ell^{\pm} + 2j + E_T^{\rm miss}$ final state analysis carried out by the ATLAS collaboration in Ref. [120]. For the EW $W^{\pm}W^{\pm}jj$ process we obtain 64 events with 36.1 fb^{-1} of integrated luminosity at $\sqrt{s} = 13$ TeV. The corresponding signal yield prediction by the ATLAS collaboration is 60 ± 11. For different light lepton flavor combination channels also, we agree with the ATLAS prediction within the error bars.

We finish the discussion on our simulation set-up with one final comment on SM background generation. For fast computation, we generate the WZ background with exactly two partons only at $\mathcal{O}(\alpha_s^4\alpha_{\rm EW}^4)$ for our analysis. We do not generate the above background inclusively and do not perform any jet-matching. However, we did check that after VBF cuts the $WZjj$ cross section is within 10% of the inclusive WZ+jets cross section. In contrast, both the EW and QCD same-sign W pair is produced at the LHC in association with two partons at LO and do not require inclusive generation.

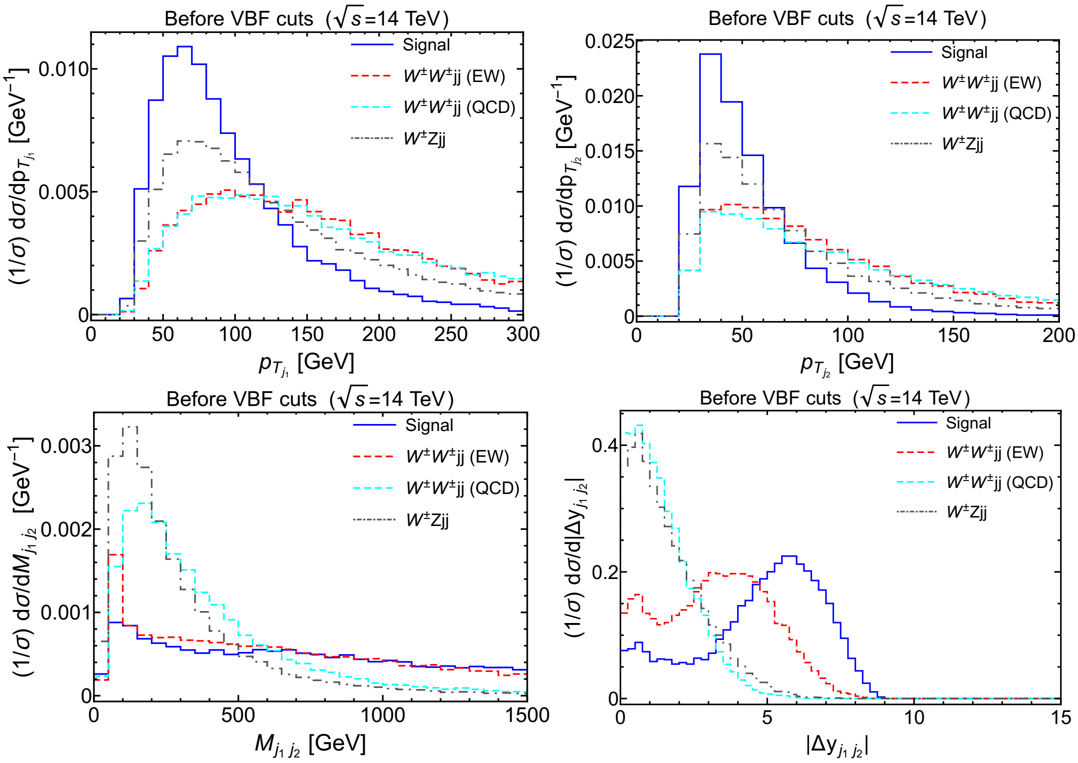

Figure 7. Jet kinematic distributions of the signal and SM backgrounds $W^{\pm}W^{\pm}jj$ (EW), $W^{\pm}W^{\pm}jj$ (QCD) and $W^{\pm}Zjj$ (QCD+EW) before VBF cuts. The top left, and right panels are respectively for the p_T distributions of the leading jet j_1 and the sub-leading jet j_2, and the lower left and right panels are respectively for the invariant mass $M_{j_1 j_2}$ and the rapidity separation $|\Delta y_{j_1 j_2}|$ of the two jets.

3.2 Selection cuts and cross sections

Next, using the reconstructed leptons and jets from `Delphes` we list the selection cuts used in our $\ell^{\pm}\ell^{\pm} + 2j + E_T^{\rm miss}$ study.

1. *Exactly same-sign dilepton + $\geq$ 2 jets*: We select exactly a pair of same-sign dilepton with additional criteria that they must be separated by a distance $\Delta R_{\ell_1 \ell_2} > 0.3$ and must have an invariant mass $m_{\ell_1 \ell_2} > 20$ GeV. Electrons are required to be outside the calorimeter transition region ($1.37 < |\eta_e| < 1.52$). To avoid additional background contributions from electron charge mis-reconstruction in di-electron events, we restrict electrons within $|\eta_e| < 1.37$ for such events, and discard events with $|m_{e_1 e_2} - m_Z| < 15$ GeV. We then require at least two jets in the selected event with $p_{T_j} > 20$ GeV and $|\eta_j| < 4.5$.

2. *VBF cuts*: As mentioned before, a VBF event is characterized by two high-p_T forward jets with large invariant mass and large separation in rapidity. Our signal is strictly produced by same-sign W fusion along with the $W^{\pm}W^{\pm}jj$ (EW) background. In contrast, the di-jet invariant mass of QCD backgrounds peaks at smaller values and they are not widely separated in $|\Delta y_{j_1 j_2}|$, as can be seen in the lower left and right

panels of Fig. 7. In contrast, the p_T distributions of the leading jet j_1 and the subleading jet j_2 for the SM backgrounds tend to be flatter than those for the signal, as shown in the top left and right panels of Fig. 7. We impose $p_{T_{j_1}} > 65$ GeV, $p_{T_{j_2}} > 35$ GeV, $m_{j_1 j_2} > 500$ GeV, and $|\Delta y_{j_1 j_2}| > 2$ to select VBF topology. On an interesting note, although both the signal and $W^\pm W^\pm jj$ (EW) background are predominantly produced by same-sign W fusion, their $|\Delta y_{j_1 j_2}|$ distributions do not peak at the same value. We attribute this difference to the contamination of $W^\pm W^\pm jj$ (EW) production by non-VBF processes. On the other hand, the signal production is strictly VBF.

3. *b-jet veto*: Although we do not simulate same-sign dilepton backgrounds arising from heavy-flavor hadron decays, we include b-veto in our cut strategy following Ref. [120] to suppress such backgrounds.

4. $E_T^{\rm miss}$ cut: As the leptonic scalar ϕ decays invisibly into neutrinos, the missing transverse energy $E_T^{\rm miss}$ tends to be slightly larger in the signal than in backgrounds. The $E_T^{\rm miss}$ distributions for the signal and backgrounds are shown in the lower left panel of Fig. 8, before VBF cuts. We impose a nominal $E_T^{\rm miss}$ cut of 30 GeV.

5. *Lepton p_T cuts*: In the SM, the charged leptons from the W boson decay have a peak at around $\sim m_W/2$. On the other hand, if a ϕ scalar is produced from a W fusion process, it tends to be soft and most of the energy of the system is more likely to be carried by the leptons. As a result, the signal lepton p_T distribution is much flatter and peaks around $\sim 2m_W$, as can be seen in the top panels of Fig. 8. We employ $p_{T_{\ell_1}} > 150$ GeV and $p_{T_{\ell_2}} > 90$ GeV to reduce $W^\pm W^\pm jj$ (EW) and $W^\pm Zjj$ backgrounds by an order of magnitude.

6. *$|\Delta\phi_{\ell_1, E_T^{miss}}|$ cut*: Finally, we use $|\Delta\phi_{\ell_1, E_T^{\rm miss}}| > 1.8$ to enhance the signal-to-background ratio, and that leads to a signal yield comparable to both $W^\pm W^\pm jj$ (EW) and $W^\pm Zjj$ backgrounds. This cut is very effective due to different origins of $E_T^{\rm miss}$ in the signal and the $W^\pm W^\pm jj$ (EW) background. While in the above background both the leptons and $E_T^{\rm miss}$ are coming from W boson decays, for the signal the $E_T^{\rm miss}$ is arising from ϕ decay and leptons are emitted by incoming virtual W bosons, which leads to different azimuthal angle correlation between them. This cut is very effective in suppressing the $W^\pm Zjj$ background as well. The $|\Delta\phi_{\ell_1, E_T^{\rm miss}}|$ distributions are shown in the lower right panel of Fig. 8.

The cross sections after each set of cuts are shown in Table 2 for both the signal and SM backgrounds we considered. We show the cut-flow for $m_\phi = 1$ GeV case with the couplings $|\lambda_{\alpha,\beta}| = 1\,(\alpha, \beta = e, \mu)$. The contribution from QCD $W^\pm W^\pm jj$ is negligible after all the cuts. However, both EW $W^\pm W^\pm jj$ and $W^\pm Zjj$ survive, with background rates comparable to the expected signal rate when we apply the specific cuts $p_{T_{\ell_1}} > 150$ GeV, $p_{T_{\ell_2}} > 90$ GeV and $|\Delta\phi_{\ell_1, E_T^{\rm miss}}| > 1.8$ in Table 2. We repeat the above analysis for a number of benchmark points with m_ϕ in the range [100 MeV, 246 GeV]. Since we are selecting a highly boosted system by using VBF topological cuts, the cut-efficiencies of all the cuts

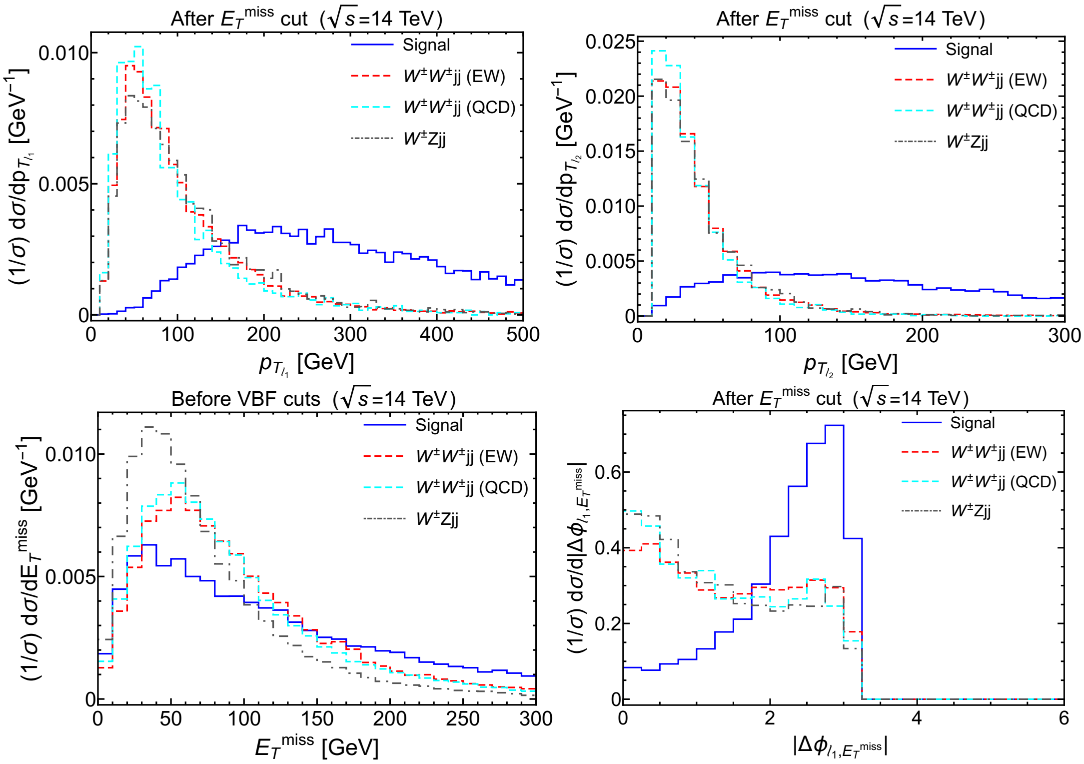

Figure 8. Kinematic distributions of the signal and SM backgrounds $W^\pm W^\pm jj$ (EW), $W^\pm W^\pm jj$ (QCD) and $W^\pm Zjj$ after the E_T^{miss} cut. The top left and right panels are respectively for the p_T distributions of the leading lepton ℓ_1 and the sub-leading lepton ℓ_2, and the lower left and right panels respectively for the missing transverse energy E_T^{miss} and the angular separation $|\Delta\phi_{\ell_1 E_T^{\text{miss}}}|$. Only the E_T^{miss} distribution is shown before VBF cuts.

shown in Table 2 show a weak dependence on m_ϕ. It is interesting to note that even if the scalar mass $m_\phi < 100$ MeV, the production cross sections and the $\lambda_{\alpha\beta}$ sensitivities will remain unchanged. For such light scalars there is no other direct limit from the LHC, although the low-energy high-precision constraints are much more stringent. We do not explore ϕ masses beyond the EW scale of $v_{\text{EW}} \simeq 246$ GeV since the effective Lagrangian of Eq. (1.1) may not be valid in that regime.

In Table 3 we present event yields in different lepton flavor combinations $e^\pm e^\pm$, $e^\pm\mu^\pm$ and $\mu^\pm\mu^\pm$ for both the signal (with $m_\phi = 1$ GeV) and SM backgrounds at 14 TeV LHC with 3 ab^{-1} of integrated luminosity. As we mentioned before, $|\lambda_{\alpha,\beta}|$ $(\alpha, \beta = e, \mu)$ are set to be 1. If we switch on couplings involving τ leptons as well we can get $\sim 15\%$ enhancement on the signal yield. In Table 3 we also calculate the significance of the signal in different channels for 0% and 10% systematic errors on the background estimation, using the metric $\sigma_{S/B} = S/\sqrt{S + B + (\epsilon_B B)^2}$. Here S and B are signal and background event yields in a particular final state, respectively, and ϵ_B is the percentage systematic error on the background estimation.

Table 2. Cut-flow table of the signal, with $m_\phi = 1$ GeV, and SM backgrounds $W^\pm W^\pm jj$ (EW), $W^\pm W^\pm jj$ (QCD) and $W^\pm Zjj$ at 14 TeV LHC. We decay $W^\pm\,(Z)$ boson to $\ell^\pm\nu\,(\ell^+\ell^-)$, where $\ell = e, \mu, \tau$ during generation. In contrast, for the signal only $\ell = e, \mu$ are considered. The couplings $|\lambda_{\alpha,\beta}|\,(\alpha, \beta = e, \mu)$ are set to be 1. Note that the particular cuts in the last two rows can suppress very effectively the SM backgrounds.

Cut selection	**Signal** [fb]	$W^\pm W^\pm jj$ (EW) [fb]	$W^\pm W^\pm jj$ (QCD) [fb]	$W^\pm Zjj$ [fb]
Production	0.782	39.0	34.5	594
exactly 2ℓ: $p_{T_{\ell_{1,2}}} > 10$ GeV, $\lvert\eta_{\ell_{1,2}}\rvert < 2.5$, $m_{\ell_1\ell_2} > 20$ GeV, $\Delta R_{\ell_1\ell_2} > 0.3$	0.530	9.26	5.65	177
same-sign dilepton	0.529	9.26	5.65	44.5
for di-electron events: $\lvert\eta_{e_1,e_2}\rvert > 1.37$, $\lvert m_{e_1e_2} - m_Z\rvert < 15$ GeV vetoed	0.476	7.90	4.71	36.5
≥ 2 jets: $p_{T_{j_{1,2}}} > 20$ GeV, $\lvert\eta(j_{1,2})\rvert < 4.5$	0.397	7.46	4.51	33.7
VBF cuts: $p_{T_{j_1}} > 65$ GeV, $p_{T_{j_2}} > 35$ GeV, $m_{j_1j_2} > 500$ GeV, $\lvert\Delta y_{j_1j_2}\rvert > 2$	0.165	4.08	0.502	3.42
b-jet veto	0.158	3.77	0.441	3.03
$E_T^{\text{miss}} > 30$ GeV	0.143	3.41	0.399	2.58
$p_{T_{\ell_1}} > 150$ GeV, $p_{T_{\ell_2}} > 90$ GeV	0.108	0.217	0.017	0.176
$\lvert\Delta\phi_{\ell_1,E_T^{\text{miss}}}\rvert > 1.8$	0.084	0.088	0.004	0.059

Table 3. Event yields in different lepton flavor combination channels $e^\pm e^\pm$, $e^\pm\mu^\pm$ and $\mu^\pm\mu^\pm$ for both the signal and SM backgrounds at 14 TeV LHC with 3 ab^{-1} of integrated luminosity. For the signal we set $m_\phi = 1$ GeV and $|\lambda_{\alpha,\beta}| = 1$ (with $\alpha, \beta = e, \mu$). We consider systematic errors of 0% and 10% on the background events only.

Channels		$e^\pm e^\pm$	$e^\pm\mu^\pm$	$\mu^\pm\mu^\pm$	**Total**
Signal		40	129	84	253
$W^\pm W^\pm jj$ (EW)		37	137	89	263
$W^\pm W^\pm jj$ (QCD)		2	9	2	13
$W^\pm Zjj$		29	94	54	177
Total background		68	240	145	453
Significance	syst. error 0%	3.87	6.73	5.53	9.53
	syst. error 10%	3.24	4.21	4.00	4.83

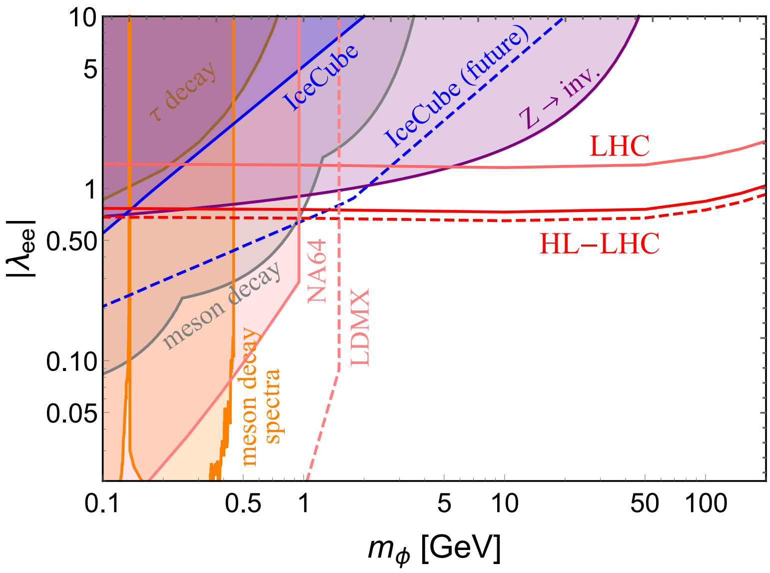

Figure 9. Prospects of the coupling $|\lambda_{ee}|$ as a function of the scalar mass m_ϕ at 14 TeV LHC with luminosity of 300 fb^{-1} (solid thin red line) and HL-LHC with 3 ab^{-1} and with systematic errors of 10% (solid thick red line) and 0% (dashed thick red line). Also shown are the low-energy limits (cf. Table 1) from meson decay (gray), τ decay (brown), heavy neutrino searches in meson decay spectra (orange), invisible Z decay (purple), light DM searches in NA64 (pink) and the prospects at LDMX (dashed pink), the current IceCube limits on neutrino–neutrino interactions (blue) and prospects (dashed blue). All the shaded regions are excluded.

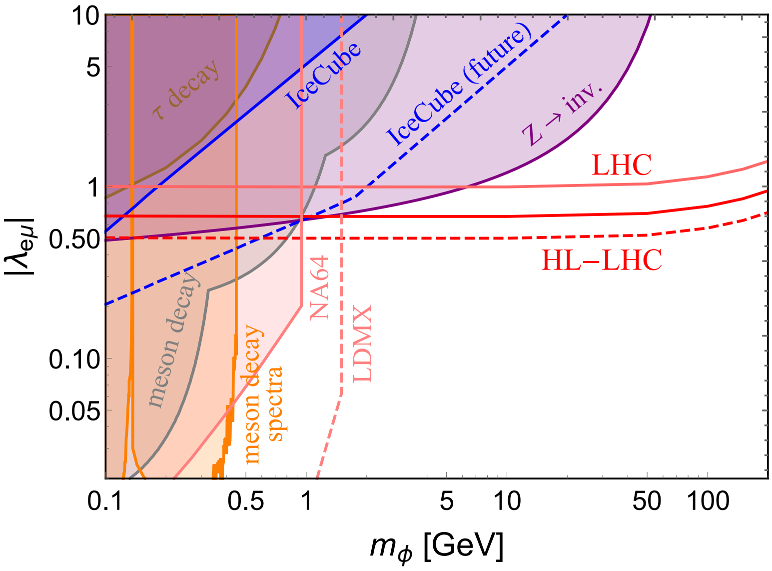

Figure 10. The same as in Fig. 9, but for the coupling $|\lambda_{e\mu}|$.

3.3 Prospects

The prospects of $\lambda_{ee,\,e\mu,\,\mu\mu}$ at the LHC and HL-LHC are shown respectively in Figs. 9, 10 and 11. The dashed thick red lines are for the most optimistic case at the 14 TeV HL-LHC

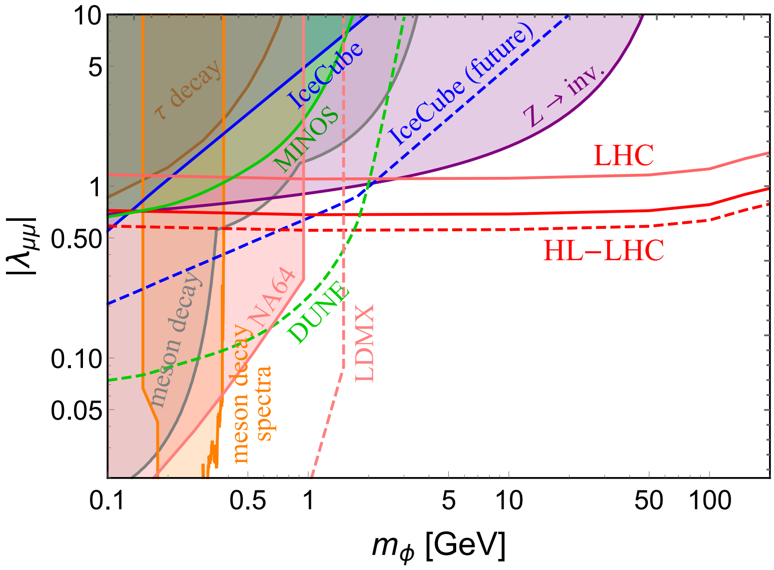

Figure 11. The same as in Fig. 9, but for the coupling $|\lambda_{\mu\mu}|$. Here we also show the limit on $|\lambda_{\mu\mu}|$ from MINOS (green) and prospect at DUNE (dashed green).

Table 4. Summary of the 95% C.L. LHC and HL-LHC sensitivities to the couplings $|\lambda_{\alpha\beta}|$ in our leptonic scalar case with $m_\phi \lesssim 50$ GeV [cf. Figs. 9–11]. Results with zero and a 10% systematic error are listed.

Collider		$\lvert\lambda_{ee}\rvert$	$\lvert\lambda_{e\mu}\rvert$	$\lvert\lambda_{\mu\mu}\rvert$
LHC	syst. error 0%	1.35	0.95	1.07
	syst. error 10%	1.38	1.00	1.13
HL-LHC	syst. error 0%	0.68	0.51	0.57
	syst. error 10%	0.76	0.68	0.70

with 3 ab^{-1} integrated luminosity and without any systematic error, where the couplings $\lambda_{ee,\, e\mu,\, \mu\mu}$ can be probed respectively up to 0.68, 0.51 and 0.57 at the 95% C.L (see Table 4). With a realistic 10% systematic error, the sensitivities at the HL-LHC are slightly weaker, being respectively 0.76, 0.68 and 0.70 at the 95% C.L., denoted by the solid thick red lines. This implies that our leptonic signals are rather robust against the systematic uncertainties on the background determination. For comparison, we also show the prospects at the 14 TeV LHC with only 300 fb^{-1} integrated luminosity, which is achievable in the upcoming run within a few years. We use the same cuts above as for the HL-LHC and assume there is a 10% systematic error. The prospects are respectively 1.38, 1.00, and 1.13 at the 95% C.L. for the couplings $\lambda_{ee,\, e\mu,\, \mu\mu}$ and shown as the thin red lines in Figs. 9–11. The corresponding LHC prospects with zero systematic uncertainty are respectively 1.35, 0.95 and 1.07, as shown in Table 4 (but not shown in Figs. 9–11 since the difference is not appreciable). The slightly better sensitivity for $\lambda_{e\mu}$ is due to the doubling of the flavor combinations; see the event rates with different lepton flavors estimated in Table 3. We find that when the scalar mass is significantly smaller than the colliding energy at LHC, say $m_\phi \lesssim 50$ GeV, the sensitivities have only a weak dependence on the scalar mass, being almost flat. We also note that although the production cross section of ϕ at the LHC via VBF process starts falling for $m_\phi \gtrsim 10$ GeV as can be seen from Fig. 6, the sensitivity curves slowly drop when the scalar mass $m_\phi \gtrsim 50$ GeV only. For the ϕ mass between 10 and 50 GeV the small decrease in the production cross section is compensated by similar increase in cut-efficiencies. Above 50 GeV, improvements in cut-efficiencies can not overcome the sharp drop in cross sections.

The prospects of $\lambda_{\alpha\beta}$ at the LHC and HL-LHC are largely complementary to the low-energy constraints discussed in Section 2. To see it more clearly, we show in Figs. 9–11 the limits from meson decays (gray), τ decays (brown), heavy neutrino searches in two-body meson decay spectra (orange), the invisible Z decay (purple), neutrino-matter scattering at MINOS (green), light DM searches in NA64 (pink) and IceCube limits on new neutrino–neutrino interactions (blue). As in Figs. 2–5, all the shaded regions are excluded. Also shown are the prospects at LDMX and IceCube by the dashed pink and dashed blue lines respectively. For the coupling $\lambda_{\mu\mu}$ we have also shown the prospect from DUNE in Fig. 11 by dashed green line. One can see from Figs. 9–11 that the HL-LHC prospects of $\lambda_{ee,\, e\mu,\, \mu\mu}$ exceed all the existing limits when the scalar mass $m_\phi \gtrsim 1$ GeV. These will be the first direct collider limits on light leptonic scalars of such kind.

4 Conclusion

In this paper, we studied the neutrino non-standard interaction in a simplified framework where a (light) scalar ϕ couples exclusively to the active neutrinos. As such, it carries two units of lepton-number, and is dubbed as "leptonic scalar". The Yukawa couplings $\lambda_{\alpha\beta}$ of ϕ to neutrinos are constrained by different low-energy, high-precision data, such as the charged meson and lepton decays rates, meson decay spectra, the W and Z decay rates, neutrino beam experiments like MINOS and, in the future, DUNE, light DM searches in NA64 and LDMX, IceCube and CMB limits on new neutrino self interactions, as well as other limits which are mostly relevant to a light scalar with mass $m_\phi \lesssim 100$ MeV.

We showed that the leptonic scalar ϕ can be produced at high-energy hadron colliders like the LHC via fusion of two same-sign W bosons, i.e., $pp \to \ell_\alpha^\pm \ell_\beta^\pm jj + \phi$. As ϕ decays into neutrinos, we have the distinctive signature $pp \to \ell_\alpha^\pm \ell_\beta^\pm jj + E_T^{\rm miss}$. The predominant SM background is the electroweak vector boson scattering process $pp \to W^\pm W^\pm jj$, with sub-leading contributions from the $W^\pm Zjj$ production and QCD $W^\pm W^\pm jj$ processes. Given the presence of the scalar ϕ, the kinematic distributions of the charged leptons, jets and missing transverse energy are very different for the signal and backgrounds and can be used to effectively separate the two. Upon dedicated simulations of both signal and backgrounds, we find that for m_ϕ less than the electroweak scale, the couplings $\lambda_{ee,\, e\mu,\, \mu\mu}$ can be probed, respectively, up to 1.38, 1.00 and 1.13 at the 95% C.L. at the LHC with an integrated luminosity of 300 fb^{-1}, and down to 0.76, 0.68 and 0.70 at the HL-LHC with 3 ab^{-1} integrated luminosity; see Table 4 for a quick summary. Based on this analysis, we find that the direct constraints from the ongoing LHC would be better than all other existing constraints for $m_\phi \gtrsim 1$ GeV. Figs. 9, 10 and 11 summarize our results for the couplings $|\lambda_{\alpha\beta}|$ with $\alpha\beta = ee, e\mu, \mu\mu$ respectively. At future colliders, such as a high-energy upgrade of the LHC or a future 100 TeV pp collider, an improved sensitivity is expected. In some sense, this is a direct probe of scalar-mediated neutrino self-interactions at high-energy colliders, and is largely complementary to the constraints from the low-energy high-intensity experiments and the astrophysical and cosmological observations.

In our analysis, we introduce the neutrino coupling to the leptonic scalar ϕ via an effective dimension-six operator $(LH)(LH)\phi$ [2, 3]. There are several possible ultraviolet-completions of the effective operator. As an example, let us consider $\mathcal{L} \supset \lambda_1 LL\Delta + \lambda_2 \phi H \Delta H$, where Δ is an $SU(2)_L$ scalar triplet with a mass close to or slightly higher than the weak scale and ϕ is a singlet (see Ref. [128]). Once Δ is integrated out, the above-mentioned dimension-six operator is produced, with the naive expectation for an effective coupling $\lambda_{\rm eff} \sim \lambda_1 \lambda_2 v_{\rm EW}^2 / M_\Delta^2$. Other examples were discussed recently in Ref. [129]. Finally, the results discussed here also apply if the neutrinos are Majorana fermions under the assumption that lepton-number violating effects are very small and effectively absent at collider experiments. For example, if very heavy Majorana masses $M_{\nu^c} \gg v_{\rm EW}$ for the right-handed neutrinos are added to the SM Lagrangian (along with the neutrino Yukawa couplings), which make up the only source of lepton-number violation, then lepton-number symmetry is approximately conserved at collider energies. In this case, it is fair to assign a lepton-number-charge to ϕ and assume that its main coupling to the SM is via the dimension-six operator of interest.

Acknowledgements

We thank Kevin Kelly for useful discussion. This work was initiated at the NTN NSI workshop, supported in part by the US Neutrino Theory Network Program under Grant No. DE-AC02-07CH11359, as well as by the Department of Physics and the McDonnell Center for the Space Sciences at Washington University in St. Louis. PSBD would like to thank the Fermilab Theory Group for warm hospitality where part of this work was done. YZ would like to thank the Institute of Theoretical Physics, Chinese Academy of Sciences, the Tsung-Dao Lee Institute, and the Institute of High Energy Physics, Chinese Academy of Sciences for generous hospitality where part of this work was done. The work of AdG was supported in part by the U.S. Department of Energy under grant No. DE-SC0010143. The work of PSBD and YZ was supported in part by the U.S. Department of Energy under Grant No. DE-SC0017987 and in part by the MCSS. The work of BD was supported in part by the U.S. Department of Energy under grant No. DE-SC0010813. TG was supported by U.S. Department of Energy under grant No. DE-SC0010504. The work of TH was supported in part by the U.S. Department of Energy under grant No. DE-FG02-95ER40896 and in part by the PITT PACC. This work was partially performed at the Aspen Center for Physics, which is supported by National Science Foundation grant PHY-1607611.

A Calculations of Multi-body Decays Involving ϕ

A.1 Three-body decays $Z \to \nu_\alpha \nu_\beta \phi$ and $W \to \ell_\alpha \nu_\beta \phi$

For the decay $Z \to \nu_\alpha(p_2) + \nu_\beta(p_3) + \phi(p_1)$ with the flavor index $\alpha = e, \mu, \tau$ and $p_{1,2,3}$ the momenta of particles in the final state, the scalar ϕ can be emitted from either of two neutrino lines, and the partial width reads

$$\Gamma(Z \to \nu_\alpha \nu_\beta \phi) = \frac{g^2 |\lambda_{\alpha\beta}|^2}{12 m_Z (1+\delta_{\alpha\beta}) \cos^2\theta_W} \int \mathrm{d}\Phi_3 \left(|\mathcal{M}_1|^2 + |\mathcal{M}_2|^2 \right) , \tag{A.1}$$

with m_Z the Z boson mass, θ_W the weak mixing angle, g the coupling constant for the SM gauge group $SU(2)_L$, and the two reduced amplitudes squared are respectively

$$\begin{aligned} |\mathcal{M}_{1,2}|^2 = \frac{1}{(p_1+p_{3,2})^2} \Bigg[& 4(p_1 \cdot p_2)(p_1 \cdot p_3) - 2 m_Z^2 x_{\phi Z} (p_2 \cdot p_3) \\ & + \frac{(p_2 \cdot p_3)}{m_Z^2} \left(m_Z^2 x_{\phi Z}^2 + 2(p_1 \cdot p_{3,2}) \right)^2 \Bigg] , \end{aligned} \tag{A.2}$$

with $x_{\phi Z} = m_\phi^2 / m_Z^2$, and the three-body phase space [130]

$$\mathrm{d}\Phi_3 = \frac{m_Z^2 \Omega_2 \Omega_3}{2^{10}\pi^5} \frac{\lambda_2 (1-\lambda_2)(1-x_{\phi Z})^3}{\lambda_2(1-x_{\phi Z}) + x_{\phi Z}} \mathrm{d}\lambda_1 \mathrm{d}\lambda_2 ,$$

where $\Omega_d \equiv 2\pi^{d/2}/\Gamma(d/2)$ is the solid angle in d dimension, and $0 < \lambda_{1,2} < 1$ are the two dimensionless kinematic variables. The scalar products of momenta can be expressed as functions of m_Z, $x_{\phi Z}$ and $\lambda_{1,2}$ in the following form [130]:

$$(p_1 \cdot p_2) = \frac{m_Z^2}{2} \frac{(1-\lambda_1)(1-\lambda_2)[x_{\phi Z} + (1-x_{\phi Z})\lambda_1\lambda_2]}{\lambda_2(1-x_{\phi Z}) + x_{\phi Z}} , \tag{A.3}$$

$$(p_2 \cdot p_3) = \frac{m_Z^2}{2} \frac{\lambda_2(1-\lambda_1)(1-\lambda_2)(1-x_{\phi Z})^2}{\lambda_2(1-x_{\phi Z}) + x_{\phi Z}} , \tag{A.4}$$

$$(p_1 \cdot p_3) = \frac{m_Z^2}{2} (1-x_{\phi Z}) \lambda_2 . \tag{A.5}$$

The calculation of partial width for the W boson decay $W \to \ell_\alpha \nu_\beta \phi$ is quite similar, for which we have only one diagram, and the partial width is

$$\Gamma(W \to \ell_\alpha \nu_\beta \phi) = \frac{g^2 |\lambda_{\alpha\beta}|^2}{6 m_W} \int \mathrm{d}\Phi_3(m_W) \, |\mathcal{M}_1(m_W, x_{\phi W})|^2 , \tag{A.6}$$

with $x_{\phi W} \equiv m_\phi^2 / m_W^2$.

A.2 Four-body decays $\tau \to \ell\nu\nu\phi$

For the four-body decays $\tau \to \ell_\alpha(p_2) + \nu_\beta(p_3) + \nu_\gamma(p_4) + \phi(p_1)$ with the flavor indices $\alpha = e, \mu$ and $\beta, \gamma = e, \mu, \tau$, the scalar ϕ could couple to the ν_α and/or the ν_τ lines, depending on the flavor indices of the coupling $\lambda_{\rho\sigma}$. In particular, when $\rho = \beta = \alpha$ and

$\sigma = \gamma = \tau$ we have two diagrams, and only one for other cases. For simplicity, we neglect the charged lepton mass in the final state, and the partial width is

$$\Gamma(\tau \to \ell_\alpha \nu\nu\phi) \simeq \frac{32 G_F^2 |\lambda_{\beta\gamma}|^2}{m_\tau (1 + \delta_{\rho\beta}\delta_{\sigma\tau})} \int \mathrm{d}\Phi_4 \left(\delta_{\rho\alpha} |\mathcal{M}_1|^2 + \delta_{\sigma\tau} |\mathcal{M}_2|^2 \right) , \tag{A.7}$$

where the δ factors in the denominator account for identical neutrinos in the final state, and the reduced amplitudes squared are

$$|\mathcal{M}_1|^2 = \frac{(p_2 \cdot p_4)}{(p_1 + p_3)^2} \left[2 \, (p_2 \cdot p_4) \, p_1 \cdot (p_2 + p_3 + p_4) + m_\tau^2 x_{\phi\tau} p_3 \cdot (p_1 - p_2 - p_4) \right] , \tag{A.8}$$

$$|\mathcal{M}_2|^2 = \frac{(p_1 \cdot p_3) + (p_2 \cdot p_3) + (p_3 \cdot p_4)}{(p_1 + p_4)^2} \left[2 (p_1 \cdot p_2)(p_1 \cdot p_4) - m_\tau^2 x_{\phi\tau} (p_2 \cdot p_4) \right] , \tag{A.9}$$

with $x_{\phi\tau} \equiv m_\phi^2 / m_\tau^2$, and the four-body phase space is [130]

$$\begin{aligned} \mathrm{d}\Phi_4 &= \frac{m_\tau^4}{128} \frac{\Omega_1 \Omega_2 \Omega_3}{(2\pi)^8} \mathrm{d}\lambda_1 \mathrm{d}\lambda_2 \mathrm{d}\lambda_3 \mathrm{d}\lambda_4 \mathrm{d}\lambda_5 \\ &\times (1 - \sqrt{x_{\phi\tau}})^5 \, (\lambda_1 (1 - \lambda_2)) \, (\lambda_5 (1 - \lambda_5))^{-1/2} \\ &\times \left[(1 - \lambda_1)((1 + \sqrt{x_{\phi\tau}})^2 - \lambda_1 (1 - \sqrt{x_{\phi\tau}})^2) \right]^{1/2} , \end{aligned} \tag{A.10}$$

where $0 < \lambda_i < 1$ with $i = 1$ to 5 are the five dimensionless kinematic variables. The scalar products of momenta can be expressed as functions of m_τ, $x_{\phi\tau}$ and the λ's in the following form [130]:

$$(p_1 \cdot p_2) = E_2 \left(E_1 - \sqrt{E_1^2 - x_{\phi\tau} m_\tau^2} \cos\theta_1 \right) , \tag{A.11}$$

$$(p_1 \cdot p_3) = \frac{1}{2} \left[(s_{13}^+ - s_{13}^-) \lambda_5 + s_{13}^- - m_\tau^2 x_{\phi\tau} \right] , \tag{A.12}$$

$$(p_1 \cdot p_4) = E_1 \sqrt{s_{234}} - (p_1 \cdot p_2) - (p_1 \cdot p_3) , \tag{A.13}$$

$$(p_2 \cdot p_3) = \frac{1}{2} m_\tau^2 (1 - \sqrt{x_{\phi\tau}})^2 \lambda_1 (1 - \lambda_2) \lambda_4 , \tag{A.14}$$

$$(p_2 \cdot p_4) = E_2 \sqrt{s_{234}} - (p_2 \cdot p_3) , \tag{A.15}$$

$$(p_3 \cdot p_4) = \frac{1}{2} m_\tau^2 (1 - \sqrt{x_{\phi\tau}})^2 \lambda_1 \lambda_2 , \tag{A.16}$$

where

$$E_1 = \frac{m_\tau^2 (1 - x_{\phi\tau}) - s_{234}}{2\sqrt{s_{234}}} , \tag{A.17}$$

$$E_2 = \frac{1}{2} m_\tau \sqrt{\lambda_1} (1 - \lambda_2)(1 - \sqrt{x_{\phi\tau}}) , \tag{A.18}$$

$$s_{234} = m_\tau^2 (1 - \sqrt{x_{\phi\tau}})^2 \lambda_1 , \tag{A.19}$$

$$\cos\theta_1 = 2\lambda_3 - 1 , \tag{A.20}$$

$$\begin{aligned} s_{13}^\pm = m_\tau^2 \Bigg[& x_{\phi\tau} + \frac{1}{2} (1 - \sqrt{x_{\phi\tau}}) \left[(\lambda_2 (1 - \lambda_4) + \lambda_4) \left(1 + \sqrt{x_{\phi\tau}} - \lambda_1 (1 - \sqrt{x_{\phi\tau}}) \right) \right. \\ & \left. \pm (\lambda_2 (1 - \lambda_4) - \lambda_4) (1 - 2\lambda_3) \sqrt{(1 - \lambda_1) \left((1 + \sqrt{x_{\phi\tau}})^2 - \lambda_1 (1 - \sqrt{x_{\phi\tau}})^2 \right)} \right] \Bigg] \end{aligned}$$

$$\pm 2(1-\sqrt{x_{\phi\tau}})\sqrt{\lambda_2(1-\lambda_3)\lambda_3(1-\lambda_4)\lambda_4(1-\lambda_1)\left((1+\sqrt{x_{\phi\tau}})^2-\lambda_1(1-\sqrt{x_{\phi\tau}})^2\right)}\Bigg] . \tag{A.21}$$

References

[1] M. Tanabashi *et al.* [Particle Data Group], Phys. Rev. D **98**, no. 3, 030001 (2018).

[2] J. M. Berryman, A. de Gouvêa, K. J. Kelly and Y. Zhang, Phys. Rev. D **97**, no. 7, 075030 (2018) [arXiv:1802.00009 [hep-ph]].

[3] K. J. Kelly and Y. Zhang, Phys. Rev. D **99**, no. 5, 055034 (2019) [arXiv:1901.01259 [hep-ph]].

[4] H. M. Georgi, S. L. Glashow and S. Nussinov, Nucl. Phys. B **193**, 297 (1981).

[5] M. Doi, T. Kotani and E. Takasugi, Prog. Theor. Phys. Suppl. **83**, 1 (1985).

[6] R. Arnold *et al.* [NEMO-3 Collaboration], Phys. Rev. D **89**, no. 11, 111101 (2014) [arXiv:1311.5695 [hep-ex]].

[7] R. Arnold *et al.* [NEMO-3 Collaboration], Phys. Rev. D **92**, no. 7, 072011 (2015) [arXiv:1506.05825 [hep-ex]].

[8] R. Arnold *et al.* [NEMO-3 Collaboration], Phys. Rev. D **93**, no. 11, 112008 (2016) [arXiv:1604.01710 [hep-ex]].

[9] R. Arnold *et al.* [NEMO-3 Collaboration], Phys. Rev. D **94**, no. 7, 072003 (2016) [arXiv:1606.08494 [hep-ex]].

[10] R. Arnold *et al.* [NEMO-3 Collaboration], Eur. Phys. J. C **78**, no. 10, 821 (2018) [arXiv:1806.05553 [hep-ex]].

[11] R. Arnold *et al.* [NEMO-3 Collaboration], Eur. Phys. J. C **79**, no. 5, 440 (2019) [arXiv:1903.08084 [nucl-ex]].

[12] A. Gando *et al.* [KamLAND-Zen Collaboration], Phys. Rev. C **86**, 021601 (2012) [arXiv:1205.6372 [hep-ex]].

[13] J. B. Albert *et al.* [EXO-200 Collaboration], Phys. Rev. D **90**, no. 9, 092004 (2014) [arXiv:1409.6829 [hep-ex]].

[14] M. Agostini *et al.* [GERDA Collaboration], Eur. Phys. J. C **75**, no. 9, 416 (2015) [arXiv:1501.02345 [nucl-ex]].

[15] W. Y. Keung and G. Senjanović, Phys. Rev. Lett. **50**, 1427 (1983).

[16] A. Atre, T. Han, S. Pascoli and B. Zhang, JHEP **0905**, 030 (2009) [arXiv:0901.3589 [hep-ph]].

[17] F. F. Deppisch, P. S. B. Dev and A. Pilaftsis, New J. Phys. **17**, no. 7, 075019 (2015) [arXiv:1502.06541 [hep-ph]].

[18] A. de Gouva and A. Kobach, Phys. Rev. D **93**, no. 3, 033005 (2016) [arXiv:1511.00683 [hep-ph]].

[19] Y. Cai, T. Han, T. Li and R. Ruiz, Front. in Phys. **6**, 40 (2018) [arXiv:1711.02180 [hep-ph]].

[20] A. P. Lessa and O. L. G. Peres, Phys. Rev. D **75**, 094001 (2007) [hep-ph/0701068].

[21] P. S. Pasquini and O. L. G. Peres, Phys. Rev. D **93**, no. 5, 053007 (2016) Erratum: [Phys. Rev. D **93**, no. 7, 079902 (2016)] [arXiv:1511.01811 [hep-ph]].

[22] A. Abada *et al.* [FCC Collaboration], Eur. Phys. J. ST **228**, no. 5, 1109 (2019).

[23] A. Abada *et al.* [FCC Collaboration], Eur. Phys. J. ST **228**, no. 4, 755 (2019).

[24] M. Ahmad *et al.*, IHEP-CEPC-DR-2015-01, IHEP-TH-2015-01, IHEP-EP-2015-01.

[25] E. Cortina Gil *et al.* [NA62 Collaboration], Phys. Lett. B **778**, 137 (2018) [arXiv:1712.00297 [hep-ex]].

[26] D. Banerjee *et al.* [NA64 Collaboration], arXiv:1906.00176 [hep-ex].

[27] T. Akesson *et al.* [LDMX Collaboration], arXiv:1808.05219 [hep-ex].

[28] K. Ioka and K. Murase, PTEP **2014**, no. 6, 061E01 (2014) [arXiv:1404.2279 [astro-ph.HE]].

[29] K. C. Y. Ng and J. F. Beacom, Phys. Rev. D **90**, no. 6, 065035 (2014) Erratum: [Phys. Rev. D **90**, no. 8, 089904 (2014)] [arXiv:1404.2288 [astro-ph.HE]].

[30] C. E. Picciotto *et al.*, Phys. Rev. D **37**, 1131 (1988).

[31] J. Heintze *et al.*, Nucl. Phys. B **149**, 365 (1979).

[32] A. V. Artamonov *et al.* [E949 Collaboration], Phys. Rev. D **94**, no. 3, 032012 (2016) [arXiv:1606.09054 [hep-ex]].

[33] D. I. Britton *et al.*, Phys. Rev. D **46**, R885 (1992).

[34] A. Aguilar-Arevalo *et al.* [PIENU Collaboration], Phys. Rev. D **97**, no. 7, 072012 (2018) [arXiv:1712.03275 [hep-ex]].

[35] T. Yamazaki *et al.*, Conf. Proc. C **840719**, 262 (1984).

[36] A. V. Artamonov *et al.* [E949 Collaboration], Phys. Rev. D **91** (2015) no.5, 052001 Erratum: [Phys. Rev. D **91** (2015) no.5, 059903] [arXiv:1411.3963 [hep-ex]].

[37] A. S. Sadovsky *et al.* [OKA Collaboration], Eur. Phys. J. C **78**, no. 2, 92 (2018) [arXiv:1709.01473 [hep-ex]].

[38] C. Lazzeroni *et al.* [NA62 Collaboration], Phys. Lett. B **772**, 712 (2017) [arXiv:1705.07510 [hep-ex]].

[39] G. Bernardi *et al.*, Phys. Lett. **166B**, 479 (1986).

[40] G. Bernardi *et al.*, Phys. Lett. B **203**, 332 (1988).

[41] A. M. Cooper-Sarkar *et al.* [WA66 Collaboration], Phys. Lett. **160B**, 207 (1985).

[42] J. Badier *et al.* [NA3 Collaboration], Z. Phys. C **31**, 21 (1986).

[43] A. Vaitaitis *et al.* [NuTeV and E815 Collaborations], Phys. Rev. Lett. **83**, 4943 (1999) [hep-ex/9908011].

[44] R. Aaij *et al.* [LHCb Collaboration], Phys. Rev. D **85**, 112004 (2012) [arXiv:1201.5600 [hep-ex]].

[45] R. Aaij *et al.* [LHCb Collaboration], Phys. Rev. Lett. **112**, no. 13, 131802 (2014) [arXiv:1401.5361 [hep-ex]].

[46] B. Shuve and M. E. Peskin, Phys. Rev. D **94**, no. 11, 113007 (2016) [arXiv:1607.04258 [hep-ph]].

[47] D. Liventsev *et al.* [Belle Collaboration], Phys. Rev. D **87**, no. 7, 071102 (2013) Erratum: [Phys. Rev. D **95**, no. 9, 099903 (2017)] [arXiv:1301.1105 [hep-ex]].

[48] J. R. Batley *et al.* [NA48/2 Collaboration], Phys. Lett. B **769**, 67 (2017) [arXiv:1612.04723 [hep-ex]].

[49] K. Abe *et al.* [T2K Collaboration], arXiv:1902.07598 [hep-ex].

[50] F. Kling and S. Trojanowski, Phys. Rev. D **97**, no. 9, 095016 (2018) [arXiv:1801.08947 [hep-ph]].

[51] A. Ariga *et al.* [FASER Collaboration], Phys. Rev. D **99**, no. 9, 095011 (2019) [arXiv:1811.12522 [hep-ph]].

[52] J. P. Chou, D. Curtin and H. J. Lubatti, Phys. Lett. B **767**, 29 (2017) [arXiv:1606.06298 [hep-ph]].

[53] D. Curtin *et al.*, arXiv:1806.07396 [hep-ph].

[54] V. V. Gligorov, S. Knapen, M. Papucci and D. J. Robinson, Phys. Rev. D **97**, no. 1, 015023 (2018) [arXiv:1708.09395 [hep-ph]].

[55] J. C. Helo, M. Hirsch and Z. S. Wang, JHEP **1807**, 056 (2018) [arXiv:1803.02212 [hep-ph]].

[56] D. Dercks, H. K. Dreiner, M. Hirsch and Z. S. Wang, Phys. Rev. D **99**, no. 5, 055020 (2019) [arXiv:1811.01995 [hep-ph]].

[57] S. Alekhin *et al.*, Rept. Prog. Phys. **79**, no. 12, 124201 (2016) [arXiv:1504.04855 [hep-ph]].

[58] C. Ahdida *et al.* [SHiP Collaboration], JHEP **1904**, 077 (2019) [arXiv:1811.00930 [hep-ph]].

[59] R. Acciarri *et al.* [DUNE Collaboration], arXiv:1512.06148 [physics.ins-det].

[60] M. Acciarri *et al.* [L3 Collaboration], Phys. Lett. B **431**, 199 (1998).

[61] R. Akers *et al.* [OPAL Collaboration], Z. Phys. C **65**, 47 (1995).

[62] D. Buskulic *et al.* [ALEPH Collaboration], Phys. Lett. B **313**, 520 (1993).

[63] B. Adeva *et al.* [L3 Collaboration], Phys. Lett. B **275**, 209 (1992) Erratum: [Phys. Lett. B **277**, 530 (1992)].

[64] G. Abbiendi *et al.* [OPAL Collaboration], Eur. Phys. J. C **52**, 767 (2007) [arXiv:0708.1311 [hep-ex]].

[65] J. Abdallah *et al.* [DELPHI Collaboration], Eur. Phys. J. C **34**, 127 (2004) [hep-ex/0403042].

[66] P. Achard *et al.* [L3 Collaboration], Phys. Lett. B **600**, 22 (2004) [hep-ex/0409016].

[67] A. Heister *et al.* [ALEPH Collaboration], Eur. Phys. J. C **38**, 147 (2004).

[68] G. Aad *et al.* [ATLAS Collaboration], JHEP **1012**, 060 (2010) [arXiv:1010.2130 [hep-ex]].

[69] ATLAS Collaboration, ATLAS-CONF-2010-051.

[70] G. Aad *et al.* [ATLAS Collaboration], Phys. Lett. B **759**, 601 (2016) [arXiv:1603.09222 [hep-ex]].

[71] M. Aaboud *et al.* [ATLAS Collaboration], Eur. Phys. J. C **77**, no. 6, 367 (2017) [arXiv:1612.03016 [hep-ex]].

[72] M. Aaboud *et al.* [ATLAS Collaboration], Eur. Phys. J. C **78**, no. 2, 110 (2018) Erratum: [Eur. Phys. J. C **78**, no. 11, 898 (2018)] [arXiv:1701.07240 [hep-ex]].

[73] S. Chatrchyan *et al.* [CMS Collaboration], JHEP **1104**, 050 (2011) [arXiv:1103.3470 [hep-ex]].

[74] S. Chatrchyan *et al.* [CMS Collaboration], JHEP **1110**, 132 (2011) [arXiv:1107.4789 [hep-ex]].

[75] S. Chatrchyan *et al.* [CMS Collaboration], Phys. Rev. Lett. **109**, 111806 (2012) [arXiv:1206.2598 [hep-ex]].

[76] S. Chatrchyan *et al.* [CMS Collaboration], Phys. Rev. D **90**, no. 3, 032004 (2014) [arXiv:1312.6283 [hep-ex]].

[77] S. Chatrchyan *et al.* [CMS Collaboration], Phys. Rev. Lett. **112**, 191802 (2014) [arXiv:1402.0923 [hep-ex]].

[78] CMS Collaboration, CMS-PAS-SMP-15-004.

[79] https://twiki.cern.ch/twiki/bin/view/LHCPhysics/LHCTopWGSummaryPlots

[80] B. Rebel and S. Mufson, Astropart. Phys. **48**, 78 (2013) [arXiv:1301.4684 [hep-ex]].

[81] P. Astier *et al.* [NOMAD Collaboration], Nucl. Phys. B **611**, 3 (2001) [hep-ex/0106102].

[82] J. Balewski *et al.*, arXiv:1412.4717 [physics.ins-det].

[83] J. P. Lees *et al.* [BaBar Collaboration], Phys. Rev. Lett. **119**, no. 13, 131804 (2017) [arXiv:1702.03327 [hep-ex]].

[84] B. Wojtsekhowski, D. Nikolenko and I. Rachek, arXiv:1207.5089 [hep-ex].

[85] B. Wojtsekhowski *et al.*, JINST **13**, no. 02, P02021 (2018) [arXiv:1708.07901 [hep-ex]].

[86] M. G. Aartsen *et al.* [IceCube Collaboration], Science **342**, 1242856 (2013) [arXiv:1311.5238 [astro-ph.HE]].

[87] M. G. Aartsen *et al.* [IceCube Collaboration], Phys. Rev. Lett. **113**, 101101 (2014) [arXiv:1405.5303 [astro-ph.HE]].

[88] M. G. Aartsen *et al.* [IceCube Collaboration], arXiv:1710.01191 [astro-ph.HE].

[89] G. Barenboim, P. B. Denton and I. M. Oldengott, Phys. Rev. D **99**, no. 8, 083515 (2019) [arXiv:1903.02036 [astro-ph.CO]].

[90] S. Hannestad, JCAP **0502**, 011 (2005) [astro-ph/0411475].

[91] N. F. Bell, E. Pierpaoli and K. Sigurdson, Phys. Rev. D **73**, 063523 (2006) [astro-ph/0511410].

[92] F. Y. Cyr-Racine and K. Sigurdson, Phys. Rev. D **90**, no. 12, 123533 (2014) [arXiv:1306.1536 [astro-ph.CO]].

[93] A. Basboll, O. E. Bjaelde, S. Hannestad and G. G. Raffelt, Phys. Rev. D **79**, 043512 (2009) [arXiv:0806.1735 [astro-ph]].

[94] M. Archidiacono and S. Hannestad, JCAP **1407**, 046 (2014) [arXiv:1311.3873 [astro-ph.CO]].

[95] L. Lancaster, F. Y. Cyr-Racine, L. Knox and Z. Pan, JCAP **1707**, no. 07, 033 (2017) [arXiv:1704.06657 [astro-ph.CO]].

[96] I. M. Oldengott, T. Tram, C. Rampf and Y. Y. Y. Wong, JCAP **1711**, no. 11, 027 (2017) [arXiv:1706.02123 [astro-ph.CO]].

[97] C. D. Kreisch, F. Y. Cyr-Racine and O. Dor, arXiv:1902.00534 [astro-ph.CO].

[98] S. E. Derenzo, Phys. Rev. **181**, 1854 (1969).

[99] R. Bayes *et al.* [TWIST Collaboration], Phys. Rev. Lett. **106**, 041804 (2011).

[100] B. Armbruster *et al.*, Phys. Rev. Lett. **81**, 520 (1998) [hep-ex/9806024].

[101] B. Armbruster *et al.*, Phys. Rev. Lett. **90**, 181804 (2003) [hep-ex/0302017].

[102] G. Arcadi, J. Heeck, F. Heizmann, S. Mertens, F. S. Queiroz, W. Rodejohann, M. Slezk and K. Valerius, JHEP **1901**, 206 (2019) [arXiv:1811.03530 [hep-ph]].

[103] A. Osipowicz *et al.* [KATRIN Collaboration], hep-ex/0109033.

[104] J. Angrik *et al.* [KATRIN Collaboration], FZKA-7090.

[105] K. Choi, C. W. Kim, J. Kim and W. P. Lam, Phys. Rev. D **37**, 3225 (1988).

[106] Y. Farzan, Phys. Rev. D **67**, 073015 (2003) [hep-ph/0211375].

[107] L. Heurtier and Y. Zhang, JCAP **1702**, no. 02, 042 (2017) [arXiv:1609.05882 [hep-ph]].

[108] G. y. Huang, T. Ohlsson and S. Zhou, Phys. Rev. D **97**, no. 7, 075009 (2018) [arXiv:1712.04792 [hep-ph]].

[109] N. Aghanim *et al.* [Planck Collaboration], arXiv:1807.06209 [astro-ph.CO].

[110] B. Ahlgren, T. Ohlsson and S. Zhou, Phys. Rev. Lett. **111**, no. 19, 199001 (2013) [arXiv:1309.0991 [hep-ph]].

[111] J. F. Beacom and N. F. Bell, Phys. Rev. D **65**, 113009 (2002) [hep-ph/0204111].

[112] J. M. Berryman, A. de Gouvêa and D. Hernández, Phys. Rev. D **92**, no. 7, 073003 (2015) [arXiv:1411.0308 [hep-ph]].

[113] R. Picoreti, M. M. Guzzo, P. C. de Holanda and O. L. G. Peres, Phys. Lett. B **761**, 70 (2016) [arXiv:1506.08158 [hep-ph]].

[114] B. Aharmim *et al.* [SNO Collaboration], Phys. Rev. D **99**, no. 3, 032013 (2019) [arXiv:1812.01088 [hep-ex]].

[115] L. Funcke, G. Raffelt and E. Vitagliano, arXiv:1905.01264 [hep-ph].

[116] M. C. Gonzalez-Garcia and M. Maltoni, Phys. Lett. B **663**, 405 (2008) [arXiv:0802.3699 [hep-ph]].

[117] R. A. Gomes, A. L. G. Gomes and O. L. G. Peres, Phys. Lett. B **740**, 345 (2015) [arXiv:1407.5640 [hep-ph]].

[118] S. Choubey, D. Dutta and D. Pramanik, JHEP **1808**, 141 (2018) [arXiv:1805.01848 [hep-ph]].

[119] S. Hannestad and G. Raffelt, Phys. Rev. D **72**, 103514 (2005) [hep-ph/0509278].

[120] M. Aaboud *et al.* [ATLAS Collaboration], arXiv:1906.03203 [hep-ex].

[121] A. M. Sirunyan *et al.* [CMS Collaboration], Phys. Rev. Lett. **120**, no. 8, 081801 (2018) [arXiv:1709.05822 [hep-ex]].

[122] J. Alwall *et al.*, JHEP **1407**, 079 (2014) [arXiv:1405.0301 [hep-ph]].

[123] R. D. Ball *et al.* [NNPDF Collaboration], JHEP **1504**, 040 (2015) [arXiv:1410.8849 [hep-ph]].

[124] T. Sjostrand, S. Mrenna and P. Z. Skands, Comput. Phys. Commun. **178**, 852 (2008) [arXiv:0710.3820 [hep-ph]].

[125] J. de Favereau *et al.* [DELPHES 3 Collaboration], JHEP **1402**, 057 (2014) [arXiv:1307.6346 [hep-ex]].

[126] P. Artoisenet, R. Frederix, O. Mattelaer and R. Rietkerk, JHEP **1303**, 015 (2013) [arXiv:1212.3460 [hep-ph]].

[127] M. Cacciari, G. P. Salam and G. Soyez, JHEP **0804**, 063 (2008) [arXiv:0802.1189 [hep-ph]].

[128] A. Dey, J. Lahiri and B. Mukhopadhyaya, JHEP **1811**, 127 (2018) [arXiv:1808.04869 [hep-ph]].

[129] N. Blinov, K. J. Kelly, G. Z. Krnjaic and S. D. McDermott, arXiv:1905.02727 [astro-ph.CO].

[130] H. M. Asatrian, A. Hovhannisyan and A. Yeghiazaryan, Phys. Rev. D **86**, 114023 (2012) [arXiv:1210.7939 [hep-ph]].